ELSEVIER

Contents lists available at ScienceDirect

Marine Chemistry

journal homepage: www.elsevier.com/locate/marchem





Dynamic manganese cycling in the northern Gulf of Mexico

Jessalyn E. Davis ^{a,*}, Rebecca S. Robinson ^b, Emily R. Estes ^c, Veronique E. Oldham ^b, Evan A. Solomon ^a, Roger P. Kelly ^b, Katherine E. Bell ^{d,e}, Joseph A. Resing ^{f,g}, Randelle M. Bundy ^a

- ^a School of Oceanography, University of Washington, Seattle, WA 98105, USA
- ^b Graduate School of Oceanography, University of Rhode Island, Narragansett, RI 02882, USA
- ^c International Ocean Discovery Program, Texas A&M University, College Station, TX 77845, USA
- ^d College of the Environment and Life Sciences, University of Rhode Island, Kingston, RI, 02881, USA
- ^e Now at College of Veterinary Medicine, Cornell University, Ithica, NY 14853, USA
- f Cooperative Institute for Climate, Ocean, and Ecosystem Studies, University of Washington, Seattle, WA 98105, USA
- ⁸ NOAA/Pacific Marine Environmental Laboratory, Seattle, WA 98115, USA

ARTICLE INFO

Keywords: Gulf of Mexico Mn(III)-L Trace metal speciation Porewater

ABSTRACT

Transport processes along the river-ocean continuum influence delivery of nutrients, carbon and trace metals from terrestrial systems to the marine environment, impacting coastal primary productivity and water quality. Although trace metal transformations have been studied extensively in the Mississippi River Delta region of the Northern Gulf of Mexico, investigations of manganese (Mn) and the presence of ligand-stabilized, dissolved manganese (Mn(III)-L) and its role in the transformation of trace elements and organic matter during riverine transport and estuarine mixing have not been considered. This study examined the chemical speciation of dissolved and particulate Mn in the water column and sediment porewaters in the Mississippi River and Northern Gulf of Mexico in March of 2021 to explore transformations in Mn speciation along the river-ocean continuum and the impact of different processes on the distribution of Mn. Total dissolved Mn concentrations were highest in the Mississippi River and decreased offshore, while Mn(III)-L contributed most to the dissolved Mn pool in near-shore waters. Porewater profiles indicated that ligand stabilization prevented dissolved Mn(III) reduction below the depth of oxygen penetration and in the presence of equimolar dissolved iron(II). Dissolved Mn(III)-L was enriched in bottom waters at all Northern Gulf of Mexico stations, and diffusive flux modelling of porewater dissolved Mn suggested that reducing sediments were a source of dissolved Mn to the overlying water column in the form of both reduced Mn(II) and Mn(III)-L. A simple box model of the Mn cycle in the Northern Gulf of Mexico indicates that Mn(III)-L is required to balance the Mn budget in this region and is an integral, and previously unconsidered, piece of the Mn cycle in the Northern Gulf of Mexico. The presence of Mn(III)-L in this system likely has an outsized impact on trace element scavenging rates, oxidative capacity, and the carbon cycle that have not been previously appreciated.

1. Introduction

Manganese (Mn) is a trace nutrient and essential element in reactions such as photosynthesis (Twining and Baines, 2013) and organic matter decomposition (Froelich et al., 1979) and consequently is a regulator of oceanic primary productivity and CO₂ uptake capacity. Mn is the metal cofactor in several metalloproteins, including O₂-evolving enzyme, superoxide dismutase, arginase and phosphotransferases (Twining and Baines, 2013) and is an important mediator of bioactive element cycles

due to its multiple oxidation states, high redox potential, and relatively high concentrations in the eutrophic zone compared to other trace metals. Particulate Mn (oxyhydr)oxides are powerful scavengers of other trace metals such as iron (Fe), copper (Cu), cobalt (Co) and zinc (Zn), and thus Mn concentrations and oxidation state can exert an important control on the solubility and bioavailability of other crucial micronutrients (Goldberg, 1954).

Mn also plays a key role in many different important reactions in seawater. Dissolved Mn(II) has been suggested to reduce nitrate (NO_3^-)

^{*} Corresponding author at: School of Oceanography, University of Washington, 1501 NE Boat Street, Seattle, WA 98105, USA. *E-mail address*: jessad@uw.edu (J.E. Davis).

to dinitrogen gas in the absence of dissolved oxygen, resulting in a loss of fixed nitrogen from seawater similar to denitrification (Luther et al., 1997). Mn-oxides can also facilitate anaerobic ammonium oxidation (Javanaud et al., 2011; Lin and Taillefert, 2014), although the mechanism underlying this process has yet to be identified. In sediments, the oxidation state of Mn is a crucial component in the redox ladder of terminal electron acceptors for organic carbon oxidation; whereby Mn is the most energetically favorable inorganic oxidant following O_2 and NO_3^- (Froelich et al., 1979).

Despite the importance of Mn in many oceanic processes, many aspects of the biogeochemical cycling of Mn are unknown. In particular, although the oxidation state of Mn dictates its chemical lability and potential reaction pathways, Mn cycling and speciation has only recently started to be fully described. Dissolved Mn has long been thought to be comprised solely of Mn(II). However, it is now known that Mn speciation is comprised of a combination of Mn(II), Mn(III), ligandbound Mn(III) (Mn(III)-L), and Mn(IV). In the current view of the Mn cycle, the chemical speciation of Mn (i.e. its oxidation state) is assumed based upon its operationally-defined physical speciation (whether it passes through a 0.2 µm filter). Until recently, dissolved Mn (<0.2 µm; dMn) was assumed to be made up entirely of Mn(II) (Barnes, 1984; Canfield et al., 2005; Hansel, 2017), while particulate Mn was assumed to be comprised of Mn(III/IV) (oxyhydr)oxides. Recent studies of riverine and coastal waters have shown that Mn(III)-L often comprise a significant portion, if not the predominant fraction, of dMn (Jones et al., 2019; Oldham et al., 2021; Oldham et al., 2020; Oldham et al., 2019; Oldham et al., 2017c; Oldham et al., 2017b; Oldham et al., 2017a; Oldham et al., 2015; Trouwborst et al., 2006). Thus, dMn includes both hexaaqua Mn(II) and Mn(III)-ligand (L) complexes. In the particulate phase (>0.2 μm), Mn is in the form of Mn(III/IV) (oxyhydr)oxides (hereby referred to as MnOx) and adsorbed Mn(II/III) complexes. This revised view of the Mn cycle considers that Mn in the form Mn(III)-L can act as both an oxidant and reductant and is an integral part of the Mn cycle.

The ability of dMn to act as both an oxidant or reductant has important implications for biogeochemical cycling of trace elements and carbon. For example, Mn(III)-L is a powerful oxidant that can oxidize organic carbon to CO2 in laboratory studies, suggesting that Mn(III)-L reduction could be an important mechanism for carbon transformations in the marine environment (Kostka et al., 1995). Mn(III)-L can also inhibit the formation of MnO_x (Oldham et al., 2021), suggesting that metals which adsorb to MnO_x surfaces may be less scavengingprone in waters with abundant Mn(III)-L. The ligands that bind Mn(III) can also complex Fe(III) in laboratory studies (Parker et al., 2007; Owings et al., 2021) and these Mn(III)-L complexes can have higher stabilities than their Fe(III)-L counterparts (Luther et al., 2015). Competition between Mn and Fe for the same ligand pool could impact the solubility and bioavailability of Fe. In most studies to date that examined the speciation of dMn, Mn(III)-L complexes were shown to constitute a major fraction (up to 100 %) of dMn (Jones et al., 2020; Jones et al., 2019; Jones and Tebo, 2021; Oldham et al., 2021; Oldham et al., 2020; Oldham et al., 2019; Oldham et al., 2017c; Oldham et al., 2017b; Oldham et al., 2017a; Oldham et al., 2015; Thibault de Chanvalon et al., 2023; Thibault de Chanvalon et al., 2022; Thibault de Chanvalon and Luther, 2019; Trouwborst et al., 2006; Yakushev et al., 2009). Although Mn(III)-L is clearly a substantive portion of the dMn in many environments, the controls on the chemical speciation of Mn from a source to sink perspective and across gradients in oxygen, salinity, and organic carbon composition are still unresolved.

The Northern Gulf of Mexico (NGoM) is a dynamic estuarine system that is ideal for studying changes in Mn speciation across large gradients in organic matter inputs, salinity, and dissolved oxygen concentrations. The NGoM is primarily fed by the Mississippi-Atchafalaya River System, which contains six unique subbasins that encompass 41 % of land area of the continental United States (Turner, 2022). The NGoM receives particularly large loads of nutrients (Rabalais et al., 2001), particles

(Turner et al., 2007), and organic carbon (Bianchi et al., 2002; Malcolm and Durum, 1976; Stolpe et al., 2010), all of which play an important role in the delivery of Mn and other trace metals to the NGoM. Dissolved organic matter (DOM) interacts with dissolved metals across this salinity gradient and plays an important role in the flocculation or the transformation of trace metals from the dissolved to the particulate phase (Boyle et al., 1974, 1977; Hedges and Keil, 1999; Moore et al., 1979). A large fraction of dissolved metals precipitate during mixing of fresh and seawater endmembers and are subsequently deposited in the sediments (Boyle et al., 1977; Hedges and Keil, 1999; Moore et al., 1979; Sholkovitz, 1976; Trefry, 1977). Metals have been shown to variably interact with different classes of organic complexing substances (Buck et al., 2015; Gledhill and Buck, 2012; Moore et al., 2021; Yamashita and Jaffé, 2008). Thus, variation in the make-up of DOM in an estuary should play a role in metal-organic interactions and ultimately the fate of these two materials.

We present a novel compilation of Mn speciation (Mn(II), Mn(III)-L, and MnO $_{\rm X}$) in the water column and sediment porewaters of the Mississippi River and NGoM. We also present dissolved Fe speciation in sediment porewaters for comparison. Our sampling campaign was conducted in several hydrographic regimes (riverine, near-shore active estuarine mixing zone, off-shore shelf-slope), with the hypothesis that the physical mixing regime in the region would impact the physiochemical speciation, transport, and ultimate fate of Mn in the NGoM. We found that incorporating Mn(III)-L into the Mn cycles of the Mississippi River and NGoM influences the rate of Mn delivery to the NGoM via diffusive sedimentary flux and riverine export pathways. Our observations support that Mn(III)-L likely plays an important role in the partitioning of Mn between the dissolved and particulate pools in this system.

2. Methods

2.1. Sample collection and processing

Seawater and sediment samples were collected in March 2021, aboard the R/V Pelican (Fig. 1; Table 1). Sediment samples were collected using an 8-position multi-corer (MC-800, Ocean Instruments) and analyzed for pH, dissolved oxygen, fixed nitrogen [NH₄⁺, NO₃⁻, NO_2^-], dMn speciation [Mn(II), weakly complexed Mn(III)-L (Mn(III)-L_W), and strongly complexed Mn(III)-L (Mn(III)-L_S)], and dissolved Fe speciation [Fe(II) and Fe(III)]. The sediment core was photographed (Fig. 1) and described prior to slicing into 0.5-3.0 cm intervals using new, acid-clean flexible polypropylene sheets rinsed with surface seawater between depth intervals. Sediment from each slice was transferred to a triple-rinsed 50 mL centrifuge tube (Falcon, Fisher Scientific) and immediately centrifuged for 20 min at 2000 rpm. Centrifuged sediment samples were then transferred to an ultra-high purity N2 filled glove bag and supernatant porewater was filtered using 0.2 µm syringe filters (nylon, Millipore) into new microcentrifuge tubes, where they remained until analysis.

Water samples were collected using a 12-position CTD rosette equipped with temperature, conductivity, pH, fluorescence, oxygen, and transmissivity sensors (SeaBird Scientific). Water samples were analyzed for dMn speciation [Mn(II), Mn(III)-L_S], particulate Mn(III/IV) (oxy) hydroxides (MnO_x), total dissolved Fe (dFe), acid-leachable particulate Fe (pFe_A), and fixed nitrogen [NH $_4^+$, NO $_3^-$, NO $_2^-$]. For dMn speciation and dissolved Fe, samples were collected directly from CTD Niskin bottles into acid-clean, triple-rinsed 50 mL Falcon tubes and immediately filtered through 0.2 μm syringe filters (nylon, Millipore) into acid-washed, triple-rinsed 15 mL Falcon tubes in our ship-based lab. Each sample was subdivided into three aliquots, two of which were reserved for dMn analysis and the last third for dFe analysis. Unfiltered aliquots were reserved for pFe_A and MnO_x analyses by direct collection from CTD Niskin bottles into acid-clean, triple-rinsed 50 mL Falcon tubes and acid-clean, triple-rinsed 1 L polycarbonate bottles, respectively.

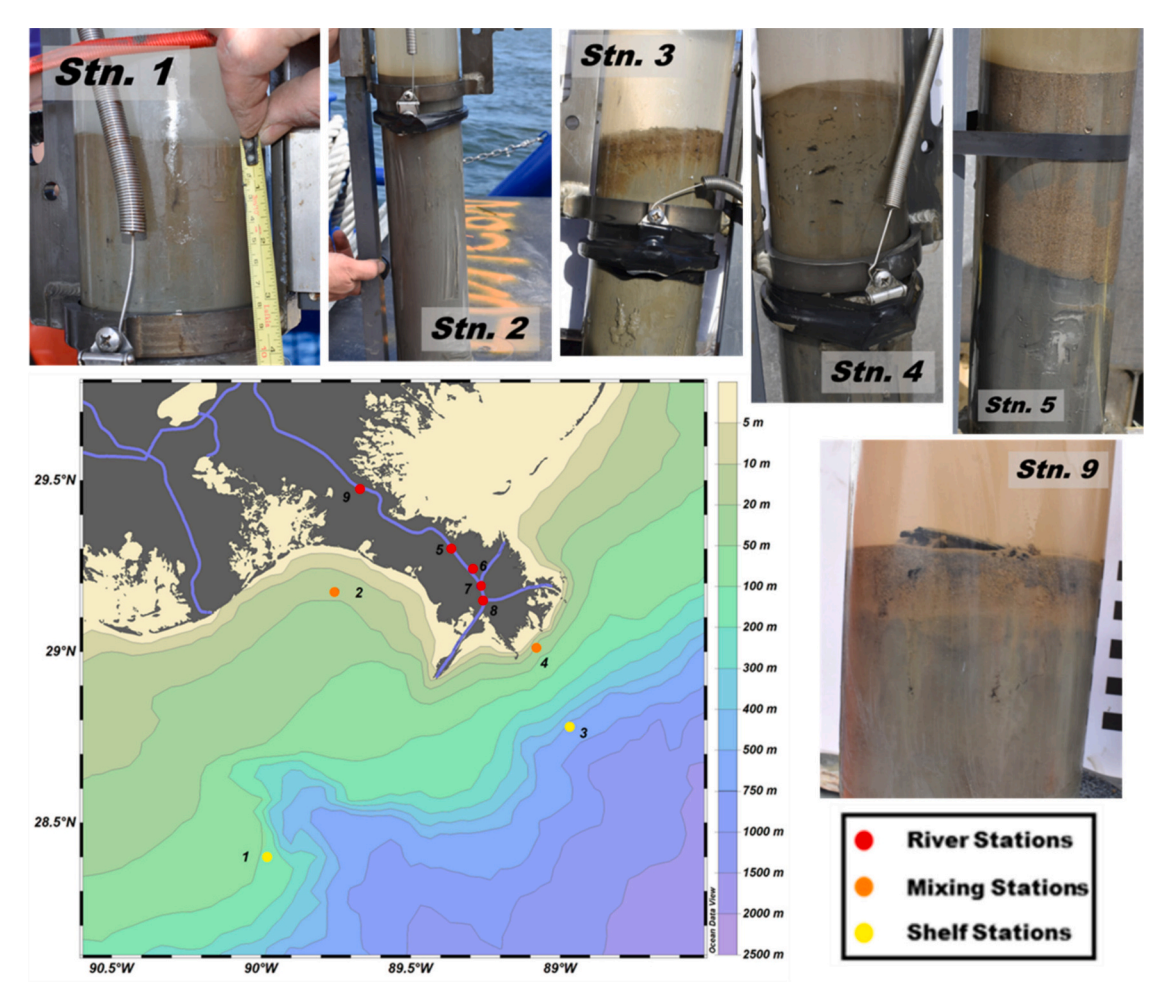


Fig. 1. a) Map of sampling locations in the Mississippi River and Gulf of Mexico. Depth contours indicate ocean bathymetry; and b) pictures of sediment cores collected at different stations highlighting the difference in sediment color and texture.

Table 1
Station location, water column depth, and corresponding surface and bottom water parameters (temperature, salinity, dissolved oxygen, and pH) for each hydrologic regime (river, mixing, shelf; detailed in section 3.1).

				Surface Water			Bottom Water					
	Station	Latitude (°N)	Longitude (°W)	Depth (m)	Temp (°C)	Salinity	Ο ₂ (μΜ)	pН	Temp (°C)	Salinity	O ₂ (μM)	pН
River	5	29.300348	89.364617	15	11.4	0.2	293.4	7.90	11.0	0.2	291.0	8.00
	6	29.237828	89.302873	19	12.2	0.2	287.2	7.78	12.2	0.2	289.3	7.77
	7	29.191120	89.267285	18	12.3	0.2	229.8	7.85	12.2	0.2	289.0	7.76
	8	29.150363	89.255640	18	12.4	0.2	243.5	7.82	12.2	0.2	288.8	7.76
	9	29.457212	89.632163	35	12.4	0.2	282.6	7.77	12.4	0.2	282.9	7.77
Mixing	2	29.170700	89.752290	15	17.6	25.5	276.2	8.30	22.0	34.0	101.3	7.99
	4	29.012265	89.082142	31	17.5	27.0	259.2	8.21	21.6	36.0	187.1	8.14
Shelf	1	28.400530	89.975355	115	22.7	36.4	209.4	8.27	18.3	36.5	137.8	8.09
	3	28.782148	89.968605	540	23.4	36.4	209.5	8.24	9.06	35.1	116.3	7.80

2.2. Dissolved porewater manganese speciation

One of the porewater aliquots was analyzed within two hours of collection for Mn(II) and weakly complexed Mn(III)-L_W, while the other was reduced with 100 μ M hydroxylamine hydrochloride (ClH₄NO; final concentration 10× the expected dMn in the sample), equilibrated overnight in the dark, and analyzed the following day for Mn(III)-L_S. All analyses for dMn speciation were conducted shipboard with the spectrophotometric porphyrin addition method described in Madison et al. (2011), which also discusses the ability of the method to differentiate between different dissolved Mn species in seawater. In brief, this method allows for the simultaneous determination of Mn(II) and Mn(III)-L_W by

using the differential reaction kinetics between Mn(II) and Mn(III)- L_W reacting with an added Cd(II)-porphyrin complex. Mn(III)- L_W is defined as a class of Mn(III)-L complexes present in the sample that are outcompeted by the porphyrin ligand ($\log K_{cond} < 13.2$). The final reduction step converts all dMn present in the sample to Mn(II), and its reanalysis quantifies dMn (Eq. (1)). The difference between [Mn(II) + Mn(III)- L_W] and [dMn] represents any Mn(III)- L_S present in the sample that could not be outcompeted by the porphyrin ligand. A kinetic constant, k_I , was determined for the substitution of Mn(II) into the Cd(II)-porphyrin complex using the reduced sample, under the assumption that all Mn present in the sample was reduced to Mn(II). This constant, k_I , was used in Eq. (2) to calculate a kinetic constant, k_2 , over time (t) for Mn(III)- L_W

ligand exchange with the porphyrin complex.

$$dMn(T) = Mn(II) + Mn(III)L_W + Mn(III)L_S$$
(1)

$$[Mn(II)] + [Mn(III)L_W] = [Mn(III) - T(4CP)P]_T$$

$$= \left[Mn(II)^{\left(1 - e^{-k_1 t}\right)}\right] + \left[Mn(III)^{\left(1 - e^{-k_2 t}\right)}\right]$$
(2)

The Mn(III)-porphyrin complex forms a sharp peak at 468 nm and has a detection limit of 50 nM in a 1 cm pathlength cell. Our setup was comprised of a 1 cm pathlength quartz cuvette and cell holder coupled to a deuterium-halogen light source and a flame UV/VIS spectrophotometer (OceanInsight). Reagents were added stepwise to the quartz cuvette as follows: 360 µL porphyrin ligand (final concentration 24 µM), 120 µL $CdCl_2$ (final concentration 48 μ M), 120 μ L imidazole borate buffer, Milli-Q® ultrapure water (variable volumes based on the [dMn] in the sample), and sufficient sample volume to fit within the analytical window of our system. The final volume of all reagents plus the sample was always 3 mL. Data were collected every 3 s, visualized using OceanViewTM software (OceanInsight) and used to quantify Mn(II) and Mn(III)-Lw. A final single absorbance scan was taken from the sample aliquot amended with hydroxylamine hydrochloride to quantify dMn and calculate Mn (III)-Ls. Blank corrected absorbance at 468 nm was converted to concentration using the molar absorptivity determined by external calibration with MnCl₂. Notably, an interference with Fe(II) has been previously reported to shift the baseline of porphyrin reagent (Owings et al., 2021). In applying this correction, it was confirmed that corrected values fall within the standard deviation of the uncorrected triplicate analyses, and thus the uncorrected values are reported throughout the manuscript.

The concentrations Mn(III)-L $_{\rm S}$ reported herein may be a slight overestimation in pore waters, due to the presence of nanoparticulate MnO $_{\rm X}$ smaller than the operational pore size used here to separate the dissolved pool (0.2 μ m) and presence of colloidal Mn in some sediment porewaters (Homoky et al., 2011). We did not separate colloidal from truly dMn (<0.02 μ m) in these samples, and did not quantify colloidal Mn in porewaters, so it is possible that some fraction of Mn(III)-L $_{\rm S}$ consists of colloidal Mn.

2.3. Dissolved water column manganese speciation

The method of Madison et al. (2011) was modified by Oldham et al. (2017c) to quantify dMn speciation in fresh and seawater samples at sub-micromolar levels. The detection limit of this method has been reported to be 0.3 nM (Oldham et al., 2017c). All analyses were performed in triplicate and standard deviations are reported for each sample. To work with sub-micromolar water column samples, reagents from above were diluted 100-fold and added to samples as described above in acid cleaned 15 mL Falcon tubes. Amended samples were heated in a 90 $^{\circ}\text{C}$ water bath for 60 mins. Samples were manually injected into a modified setup from above; the 1 cm quartz cuvette was replaced with either a 500 or 100 cm pathlength flow cell (Liquid Waveguide Capillary Cell, World Precision Instruments). The entire absorbance spectrum was saved for each sample, processed using a baseline correction software (ECDSOFT, https://puh.srce.hr/s/eAJb6M6mTpgaZos?path=ECDSOF T), and the baseline corrected absorbance at 468 nm was converted to concentration as described above for porewaters. In the water column we cannot quantify Mn(III)-LW because modifications to the method that are needed for lower detection limits cause kinetic inhibition of the reaction. Therefore, all Mn(III)-L reported for water column samples are in the form of Mn(III)-L_S. Because Mn(III)-L_S is the fraction of Mn(III)-L that cannot be outcompeted by the added porphyrin ligand (log K_{COND} > 13.2, Luther et al., 2015; Oldham et al., 2017c, Oldham et al., 2015), Mn (III)-L_S reported for the water column and for porewaters are comparable. Colloidal Mn could also be part of the dMn pool in the water column, however, even trace concentrations of calcium and magnesium cause MnO_x to precipitate (Perez-Benito et al., 1989). The colloidal

fraction of dMn in the Mississippi River water column is typically quite low (\sim 4 %; Stolpe et al., 2010), and thus we do not expect colloidal MnO $_{\rm x}$ to significantly alter our interpretation of the Mn speciation data in our dissolved water column samples.

2.4. Manganese (oxyhydr)oxides

All water column samples were run in duplicate and analyzed within 4 h of collection using the leucoberbelin blue method described by Altmann (1972) and modified by Oldham et al. (2019). Leucoberbelin blue forms a deep blue color upon oxidation by MnO $_{x}$, which can be measured via UV/Vis spectroscopy at 620 nm. In our water column samples, unfiltered waters were passed through 0.2 μ M membrane filters (Section 2.1), and the filters were transferred to acid-clean, triple-rinsed 15 mL polycarbonate Falcon tubes. The filters were amended with 0.04 % leucoberbelin blue working solution to a final concentration of 0.004 %. The dye-amended filters were placed in a refrigerator for a minimum of 90 min. After reacting, the solution was analyzed using a 1 cm quartz cuvette, and the blank corrected absorbance of the solution was measured at 620 nm using the UV/Vis setup detailed in Section 2.2.

2.5. Dissolved iron speciation in porewaters

Dissolved Fe speciation was determined in porewaters using the ferrozine method developed by Stookey (1970), which has a detection limit of 0.3 μ M (Viollier et al., 2000). Ferrozine dye solution reacts with Fe(II) to form a purple complex with a sharp absorbance peak at 562 nm, measured in a 1 cm quartz cuvette with the UV/Vis system described in Section 2.2. One filtered aliquot reserved for dissolved Fe was acidified (0.1 % Trace Metal Grade HCl, Fisher Scientific), stored for 8–12 h in the dark at room temperature and amended with 6 M ammonium acetate and 0.01 M ferrozine dye solution. Hydroxylamine hydrochloride was added to a second filtered, acidified aliquot and reacted for two hours to reduce any Fe(III) present in the sample to Fe(II), and the procedure was repeated to measure total dissolved Fe (dFe). The difference between dFe and Fe(II) yields dFe(III). The Fe(III) fraction reported here is likely a mixture of organically bound Fe(III) complexes and nanoparticulate Fe (III) species.

2.6. Dissolved inorganic nitrogen in porewaters

Dissolved nitrate (NO_3^-) and nitrite (NO_2^-) were analyzed in tandem with a Metrohm 844 UV/VIS Compact ion chromatograph. Our setup consisted of a 150 × 4.0 mm Metrosep A SUPP 8150 column with column oven temperature set to 30 $^{\circ}\text{C}$ and manual sample injection via a 0.7 mL draw of sample water through a 250 µL loop, with an eluent composition of 1 %, 0.45 µm filtered NaCl. Samples and standards (run after every fifth sample) were measured for absorbance with a flow rate of 1.5 mL min⁻¹ at 209 nm, and concentrations were determined with absorbance values via Beer's Law (Weiss, 2016). Dissolved ammonium (NH₄) was determined via Holmes et al., 1999, whereby sample water is mixed with a working reagent containing orthopthaldialdeyde (OPA), derivatizing NH₄⁺ to produce fluorescence and sodium sulfite, reducing OPA sensitivity to amino acids. Samples were incubated for 4 h and subsequently measured for fluorescence on a Trilogy Fluorometer. Samples were run in triplicate when sample volumes allowed. Relative precision was ± 10 % or better.

2.7. Dissolved oxygen and pH in porewaters

Sediment cores with at least 1 cm of overlying water were profiled with an O_2 microsensor and a pH microelectrode (Unisense). The sensors were polarized and calibrated according to Unisense user manuals. The O_2 microsensor was profiled in union with the pH microelectrode in 500 μ m intervals to 3 cm using a manual micromanipulator and the SensorTracer Suite Profiling software (Unisense). In some instances, the

core was profiled to 4 cm to obtain a more complete sediment profile. The $\rm O_2$ profile was used to determine the sediment-water interface; the point at which oxygen begins to rapidly decline was used as the sediment-water interface, and the pH profiles were adjusted with this point as "zero depth". All profiles were run in triplicate; the average and standard error of the 3 profiles were used for analysis.

2.8. Speciated manganese flux calculations from porewaters

The diffusive fluxes of Mn(II) and total Mn(III)-L (Mn(III)- L_T) from porewaters were calculated via Fick's first law (Eq. (3)), modified to account for flux due to porewater burial (Berg et al., 2019), using concentrations across the sediment-water interface and assuming transport of Mn was mainly controlled by diffusion.

$$F_{Mn(II/III)} = \varnothing D_{sed} \frac{dC_{Mn(II/III)}}{dz} + b_0 C_0$$
(3)

Here, $F_{Mn(II/III)}$ represents the flux of Mn across the sediment water interface depending on its measured oxidation state in μ mol m^{-2} d^{-1} , \varnothing represents the sediment porosity at 1 cm sediment as reported by (Allison et al., 2007), D_{sed} is the effective molecular diffusion coefficient after correcting for in situ temperature and sediment tortuosity, and $\frac{dC_{Mn}}{dz}$ represents the concentration gradient of Mn (μ mol m^{-4}). C_0 is the Mn concentration (μ mol m^{-3}) at the sediment-water interface, and b_0 is the volumetric porewater burial flux parameter which accounts for sediment compaction (Eq. (4)). The molecular diffusion constant at infinite dilution and temperature i (D_i) was corrected for in situ temperature using the Stokes-Einstein Equation (Eq. (5)) (Vanysek, 1992).

$$b_0 = \frac{\varnothing_L(1-\varnothing_0)}{(1-\varnothing_L)}s\tag{4}$$

$$D_x = \frac{T_x}{\mu_{T_x}} \times \frac{\mu_i}{T_i} \times D_i \tag{5}$$

In Eq. (5), D_x represents the molecular diffusion constant at in situ bottom water temperature T_x , and μ represents the viscosity of water at temperatures T_i and T_x . The temperature corrected diffusion constant was then corrected for sediment tortuosity by $D_{sed} = \frac{D_x}{g^2}$, where tortuosity is θ^2 and was calculated as a function of porosity: $\theta^2 = 1 - \ln(\emptyset^2)$ (Boudreau, 1997). Notably, there are no data in the literature which describe a molecular diffusion constant for Mn(III). To correct for the differing diffusion rates between the two differently charged species, the literature-reported value of D_i for Mn(II) was transformed using the ratio between $D_{Fe(II)}$: $D_{Fe(III)}$. This ratio was chosen due to the similar van der Waals atomic radii of Mn (197 pm) and Fe (194 pm). Additionally, Jones et al., 2011 report that soluble organic Fe(III)-L complexes diffuse substantially slower than ionic Fe(III). We corrected this for Mn(III)-L by repeating the model calculations using the molecular diffusion coefficient for 0.5-1 kDa humic acids (Cornel et al., 1986) instead of those used for ionic Mn(III). The values representing water column endmembers used to calculate the concentration gradient of dMn across the sediment-water interface were those measured from the deepest CTD bottle (typically no more than 1 m from the sediment surface).

3. Results

3.1. Hydrographic regimes

There were three distinct hydrological regimes present in the study area, riverine, shallow-shelf mixing, and shelf (Fig. 1). These regimes were categorized by temperature, salinity, pH, oxygen concentration and bottom depth. The riverine stations (Stations 5, 6, 7, 8 and 9) include samples collected from the mainstem of the Mississippi River and were low-salinity (S = 0.15-0.17), uniformly cold ($11.0-12.4\,^{\circ}C$), slightly acidic relative to seawater (pH = 7.86 ± 0.19 ; n=161), and

highly oxygenated (292.3 \pm 5.3 μ M, n=161). The shallow-shelf mixing stations (Stations 2 and 4) were defined by proximity to the coast, salinity ranging from riverine to open GOM with a salinity gradient with S > 5 from surface to bottom waters. Mixing stations displayed differing oxygen and temperature regimes above and below the halocline, suggesting active freshwater input and estuarine mixing. The shelf/slope stations (1 and 3) had water column stratification typical of open ocean sites. Notably, the salinities at both sites were more homogenous than the mixing sites and markedly higher than the riverine sites (S = 35.9 \pm 0.6; n=767; Fig. S1). The oxygen concentration at all of the sites considered in the study was above the hypoxic range (> 60 μ M).

3.2. Water column Mn distributions

The method used to quantify Mn(III)-L in the water columns of the Mississippi River and NGoM in this study can only capture Mn(III)-L_S due to kinetic restraints of the method at sub-micromolar concentrations of dMn (Oldham et al., 2017c). Discussions of Mn(III)-L in the water column of this study always represent Mn(III)-L_S. The concentration of dMn was variable in the Mississippi River, ranging from 64.9 to 182.6 nM (Fig. 2; Table 2), with slightly lower values (98.6 \pm 28.2 nM) upriver compared to downriver south of the first branching point of the Mississippi River (159.1 \pm 33.3 nM). The dMn values did not vary much with depth along the river, indicative of a homogenous water column, in agreement with the high river flow rate at the time of our sampling $(837,000 \pm 150,000 \text{ ft}^3 \text{ s}^{-1}, \text{ USGS})$. Organically complexed Mn(III)-L_S was 0-26 % and 0-4 % of the dMn pool in Mississippi River surface waters and bottom waters, respectively, and generally the contribution of Mn(III)-Ls to dMn decreased southward along the riverine transect. MnO_x concentrations were constant (29.0 \pm 12.3 nM) across river stations.

At the shallow-shelf mixing stations (Stations 2 and 4), the concentrations of dMn ranged from 9.4 to 191.0 nM and were highest nearshore (Fig. 3; Table 2). Depth profiles of dMn were variable at these two stations (Fig. 3). At Station 4, Mn(III)-L_S constituted 40-80 % of the dMn and dominated the dissolved pool within the halocline. Particulate MnO_x was present in very low concentrations at this station (1.6-6.3 nM), and the shape of the profile was similar to that of both Mn(III)-L_S and dMn (Fig. 3). MnO_x, dMn and Mn(III)-L_S concentrations increased to 6.3 nM, 191 nM, and 70 nM in bottom waters, respectively. The contribution of Mn(III)-Ls to dMn decreased from 70.6 \pm 9.7 % in the upper water column to 42 % at the bottom. At Station 2, the concentration of Mn(III)-Ls ranged from 0 to 94 % of the concentration of total dMn, and its contribution increased with depth. MnO_x (0 0.6-12.3 nM) was a considerably more important part of the total Mn pool, especially at the surface where the concentration of MnO_x was greater than dMn. At this location, the MnOx profile was considerably different than for dMn and Mn(III)-L_S. While MnO_x dominates the surface waters, the concentration of Mn(III)-L_S is <4 % of the total concentration of dMn. Below the surface and directly above the halocline, MnO_x decreased (12.3 to 6.8 nM) and Mn(III)-L_S increased to 93 % of dMn.

The shelf/slope stations (Stations 1 and 3) were further offshore and concentrations of dMn measured ranged from 18.6 to 93.4 nM. Concentrations of dMn were elevated at the surface and in bottom waters (Fig. 3). At Station 3, Mn(III)-L_S was slightly enriched relative to Mn(II) in the surface (54 % of dMn), and dMn shifted entirely to Mn(II) in midwaters. At depth, the contribution of Mn(III)-L_S to the dMn pool increased with depth until comprising 100 % of dMn (93.4 nM) in bottom waters. The concentration of MnO_x was consistently low (< 1 nM) throughout the entire water column (Fig. 3). In contrast to Station 3, Mn(III)-L_S contribution at Station 1 was greatest in the chlorophyll maximum (100 %) and lowest in the surface waters (23 %). MnO_x concentrations were low (< 1 nM) in the upper water column at Station 1 and were slightly enriched (1.4 nM) in the bottom waters.

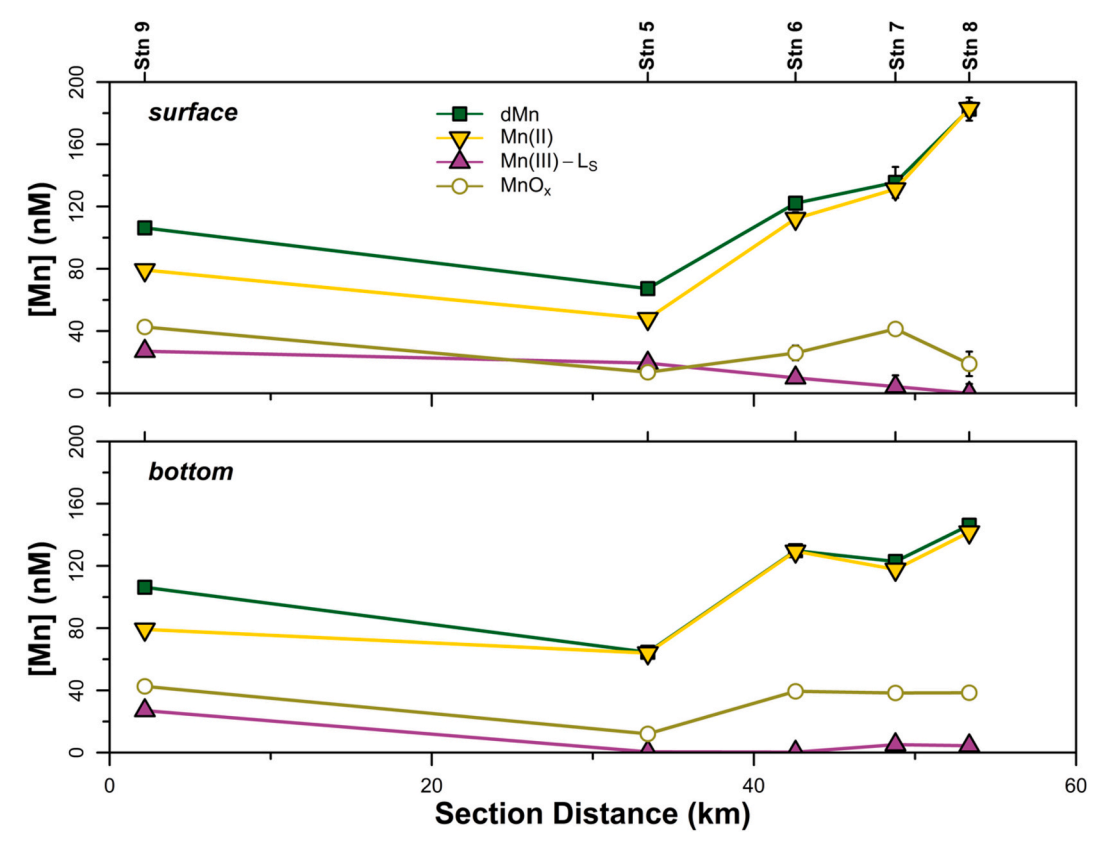


Fig. 2. Surface waters (top row) and bottom waters (bottom row) section profiles of total dissolved Mn (nM), dissolved Mn(III)- L_S (nM) and particulate Mn (nM), at all stations in the Mississippi River from our March 2021 sampling effort. Section distance represents the distance (km) from the furthest upriver Mississippi River station (Station 9).

Table 2Dissolved Mn speciation and % of Mn complexed in water column samples. All speciation measurements were conducted in triplicate.

	Station	Depth (m)	dMn (nM)	Mn(II) (nM)	Mn(III)-L (nM)	%
	-	2	67.3 ± 0.2	47.9 ± 0.7	19.4 ± 0.5	29
	5	15	64.5 ± 3.6	64.0 ± 1.9	0.5 ± 2.9	1
		1	122.2 ± 2.5	112.2 ± 4.1	9.9 ± 3.4	8
	6	17	129.8 ± 4.0	129.4 ± 1.9	0.4 ± 3.2	0
River	-	2	135.5 ± 9.9	131.2 ± 2.4	4.3 ± 7.2	3
	7	14	122.9 ± 2.0	117.7 ± 2.5	5.1 ± 2.3	4
	0	2	182.6 ± 7.4	183.0 ± 4.2	0.0 ± 6.0	0
	8	15	146.1 ± 1.3	141.7 ± 3.6	4.4 ± 2.7	3
	9	5	106.3 ± 1.5	79.2 ± 2.4	27.0 ± 2.0	25
		2	17.0 ± 0.3	17.7 ± 0.2	0.0 ± 0.0	0
		5	9.4 ± 0.1	9.0 ± 0.1	0.4 ± 0.1	4
	0	8	19.6 ± 0.6	1.4 ± 0.3	18.2 ± 0.5	93
	2	11	25.7 ± 0.2	2.2 ± 0.2	23.5 ± 0.2	92
		13	15.0 ± 0.9	1.2 ± 0.0	13.8 ± 0.6	92
Mixing		15	21.4 ± 0.2	1.1 ± 0.1	20.3 ± 0.2	95
-		2	119.8 ± 4.4	31.4 ± 1.1	88.5 ± 3.2	74
		6	48.0 ± 0.2	8.2 ± 1.2	39.8 ± 0.8	83
	4	12	32.4 ± 1.6	12.0 ± 0.3	20.3 ± 1.1	63
		15	46.5 ± 1.4	17.3 ± 0.1	29.2 ± 1.0	63
		30	191.0 ± 3.7	109.9 ± 1.5	81.2 ± 2.8	42
		2.5	37.3 ± 1.0	28.6 ± 0.6	8.7 ± 0.8	23
		20	28.3 ± 1.4	19.8 ± 0.5	8.5 ± 1.0	30
	1	55	21.0 ± 0.6	3.7 ± 2.9	17.3 ± 2.1	83
	1	65	27.8 ± 0.5	0.0 ± 0.0	27.8 ± 0.4	100
		85	18.6 ± 0.5	7.4 ± 0.4	11.2 ± 0.4	60
Shelf		113	36.9 ± 0.4	6.3 ± 0.1	30.7 ± 0.3	83
Sneir		2	35.9 ± 1.0	16.6 ± 0.6	19.3 ± 0.8	54
		80	31.6 ± 1.0	35.0 ± 0.9	0.0 ± 0.9	0
	3	120	48.1 ± 2.5	39.5 ± 0.3	8.5 ± 1.8	18
	э	162	43.3 ± 2.0	29.9 ± 0.6	13.4 ± 1.5	31
		216	26.2 ± 0.4	0.0 ± 0.0	26.2 ± 0.3	100
		513	93.4 ± 0.8	0.0 ± 0.0	93.4 ± 0.6	100

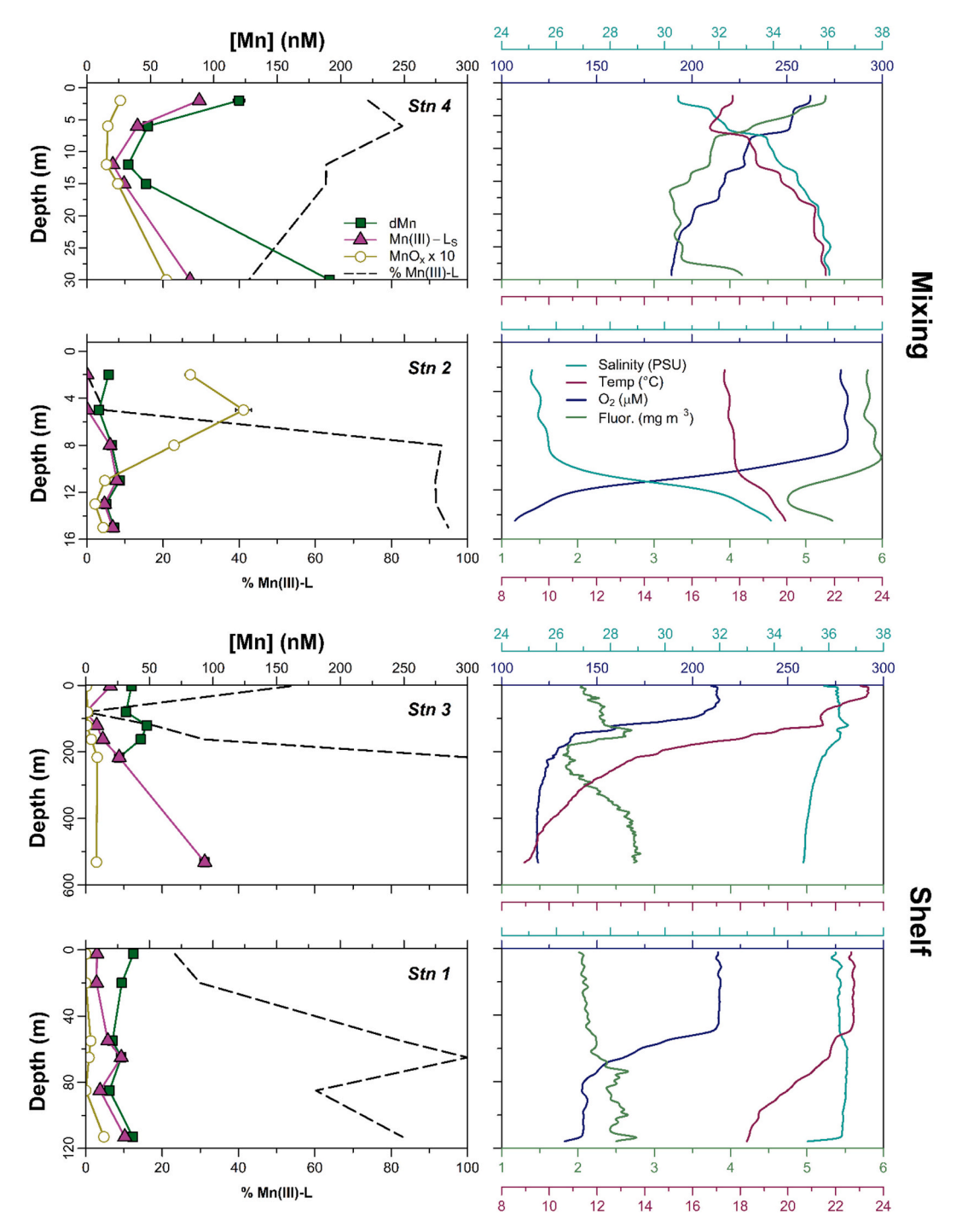


Fig. 3. Speciated water column depth profiles of dissolved and particulate Mn (nM, first column) and associated hydrographic variables (temperature (${}^{\circ}$ C), salinity, dissolved oxygen (nM), and fluorescence (mg m $^{-3}$); second column). Particulate Mn concentrations are multiplied by 10 to better visualize trends. Hydrographic variables are color coded; line colors correspond to the matching color axis.

3.3. Porewater trace metals

Sediment porewaters were enriched in dMn and dFe, relative to the water column, at all sites. Typically, the concentrations of these metals increased down core to subsurface maxima (excluding Station 5). Below the subsurface maximum at Station 9, the concentration of dMn remained relatively constant (Table 3; Fig. 4). At Stations 1, 2, 3, and 4, the concentration of dMn decreased below the subsurface maxima. At Station 5, dMn increased continually below an overlying layer of sand. The subsurface maximum of dMn and dFe in the Mississippi River sediments were lower upriver ([dMn] = 28.8 μ M and [dFe] = 44.9 μ M;

Station 9) and increased southward along the river transect ([dMn] = 531.0 μ M and [dFe] = 533.3 μ M; Station 5), similar to the trend observed in the water column. All stations had muddy sediments except Station 5; we observed a 10 cm layer of sand overlying the muddy sediments (Fig. 1). Both dMn and dFe were nondetectable in porewaters extracted from the sand layer, while NO $_3$ and NO $_2$ were enriched ([NO $_3$] = 77.5 μ M and [NO $_2$] = 1.5 μ M). Below the sand to mud transition, dMn and dFe increased concurrent with decreasing NO $_3$ and NO $_2$. Mn(III)-L and Fe(III) were enriched in the upper 5 cm of the mud layer, though generally [Mn(III)-L] > [Fe(III)] in this zone. Mn(III)-L was undetectable at 13.5 cm below the sediment surface while there

Table 3 Dissolved Mn speciation and % of Mn complexed as Mn(III)- L_W , Mn(III)- L_S and Mn(III)- L_T in sediment porewater samples. All speciation measurements were analyzed in triplicate. Zero values indicate measurements below our detection limit, while NA values represent no data available.

	Station	Depth (cm)	dMn (μM)	Mn(II) (μM)	$Mn(III)$ - L_W (μM)	%	$Mn(III)$ - L_S (μM)	%	$Mn(III)$ - L_T (μM)	%
		0.3	2.1 ± 0.1	0.8 ± 0.2	1.2 ± 0.2	55	0.2 ± 0.2	8	1.3 ± 0.4	62
		0.8	5.9 ± 0.1	3.7 ± 0.4	0.0 ± 0.0	0	2.1 ± 0.3	36	2.1 ± 0.2	36
		1.3	18.3 ± 1.4	15.1 ± 4.2	0.0 ± 0.0	0	1.7 ± 3.1	9	1.7 ± 1.7	9
	9	1.8	28.8 ± 2.8	17.3 ± 2.1	0.0 ± 0.0	0	11.5 ± 1.8	40	11.5 ± 0.4	40
	,	2.5	9.5 ± 2.2	6.2 ± 0.7	0.0 ± 0.0	0	3.3 ± 1.7	34	3.3 ± 0.6	34
		3.5	14.9 ± 1.3	5.3 ± 0.5	0.0 ± 0.0	0	9.6 ± 1.0	64	9.6 ± 0.2	64
		5.0	21.7 ± 0.0	5.6 ± 0.2	0.0 ± 0.0	0	16.1 ± 0.1	74	16.1 ± 0.0	74
River		7.0	15.3 ± 0.8	4.5 ± 0.2	0.0 ± 0.0	0	10.8 ± 0.6	71	10.8 ± 0.1	71
		10.0	53.4 ± 2.8	29.1 ± 2.5	5.7 ± 0.0	11	18.5 ± 2.7	35	24.3 ± 0.4	45
		11.5	153.6 ± 6.5	86.3 ± 3.9	32.8 ± 1.9	21	34.5 ± 5.5	22	67.3 ± 0.7	44
		12.5	214.2 ± 22.8	107.1 ± 6.3	49.4 ± 5.6	23	57.8 ± 17.2	27	107.2 ± 1.7	50
	5	13.5	296.9 ± 3.9	298.8 ± 7.9	0.0 ± 0.0	0	0.0 ± 0.0	0	0.0 ± 0.0	0
		16.0	380.6 ± 5.9	297.4 ± 6.8	32.1 ± 2.8	8	51.1 ± 6.7	13	83.1 ± 0.7	22
		17.5	479.9 ± 4.9	367.0 ± 6.4	106.4 ± 7.6	22	6.5 ± 7.9	1	112.9 ± 2.2	24
		19.5	531.0 ± 4.3	375.4 ± 5.5	100.2 ± 1.2	19	55.5 ± 5.0	10	155.6 ± 0.5	29
		0.3	NA	3.4 ± 0.5	6.1 ± 1.5	NA	NA	NA	NA	NA
		0.8	222.6 ± 8.3	30.1 ± 2.3	134.7 ± 11.4	61	57.8 ± 10.1	26	192.5 ± 1.2	86
		1.5	774.2 ± 1.2	809.9 ± 12.6	0.0 ± 0.0	0	0.0 ± 0.0	0	0.0 ± 0.0	0
	4	2.5	560.6 ± 5.8	450.6 ± 10.5	15.0 ± 2.0	3	95.0 ± 8.6	17	110.0 ± 0.7	20
	4	4.0	489.5 ± 27.1	333.4 ± 49.9	149.5 ± 69.7	31	6.7 ± 63.6	1	156.2 ± 17.9	32
		6.0	352.5 ± 24.3	298.1 ± 17.4	27.4 ± 10.6	8	27.1 ± 22.4	8	54.5 ± 3.4	15
		8.0	285.6 ± 7.1	171.0 ± 22.6	0.0 ± 0.0	0	114.6 ± 16.8	40	114.6 ± 1.1	40
		11.5	250.0 ± 10.7	239.2 ± 21.3	0.0 ± 0.0	0	10.8 ± 16.8	4	10.8 ± 3.6	4
Mixing	2	0.3	2.3 ± 0.3	0.5 ± 0.0	1.2 ± 0.0	50	0.7 ± 0.2	29	1.8 ± 0.2	79
		0.8	11.3 ± 1.7	0.0 ± 0.0	3.2 ± 0.1	28	8.1 ± 1.2	72	11.3 ± 0.3	100
		1.3	3.5 ± 1.4	2.4 ± 0.4	0.0 ± 0.0	0	1.1 ± 1.0	33	1.1 ± 0.7	33
		1.8	3.0 ± 0.5	0.0 ± 0.0	3.8 ± 0.5	100	0.0 ± 0.0	0	3.8 ± 0.2	100
		2.5	49.4 ± 3.8	42.8 ± 1.8	0.0 ± 0.0	0	6.6 ± 2.9	13	6.6 ± 0.8	13
		3.5	109.8 ± 0.6	104.0 ± 2.2	1.0 ± 1.8	1	4.8 ± 2.0	4	5.8 ± 1.4	5
		5.0	96.5 ± 2.3	52.0 ± 1.2	29.6 ± 1.2	31	14.9 ± 2.0	15	44.5 ± 0.4	46
		7.0	79.5 ± 1.4	68.7 ± 5.1	0.0 ± 0.0	0	10.8 ± 3.7	14	10.8 ± 0.8	14
		0.3	4.7 ± 0.2	3.6 ± 4.8	3.7 ± 0.2	80	0.0 ± 0.0	0	3.7 ± 0.1	80
	3	0.8	55.0 ± 1.0	53.2 ± 2.2	0.0 ± 0.0	0	1.8 ± 1.7	3	1.8 ± 0.9	3
		1.3	87.7 ± 2.6	80.7 ± 4.7	0.0 ± 0.0	0	0.0 ± 0.0	0	0.0 ± 0.0	0
		1.8	$129.3\pm.3$	125.8 ± 1.8	0.0 ± 0.0	0	0.0 ± 0.0	0	0.0 ± 0.0	0
		2.5	99.9 ± 8.8	98.7 ± 1.2	0.0 ± 0.0	0	0.0 ± 0.0	0	0.0 ± 0.0	0
Shelf		3.5	108.0 ± 2.3	107.2 ± 11.8	0.0 ± 0.0	0	0.0 ± 0.0	0	0.0 ± 0.0	0
		5.0	82.6 ± 1.1	75.2 ± 5.7	0.0 ± 0.0	0	0.0 ± 0.0	0	0.0 ± 0.0	0
	1	7.0	53.3 ± 0.4	49.2 ± 4.3	0.0 ± 0.0	0	0.0 ± 0.0	0	0.0 ± 0.0	0
		0.3	3.8 ± 1.7	1.2 ± 0.2	0.4 ± 0.1	10	2.2 ± 1.2	59	2.6 ± 0.1	69
		0.8	5.5 ± 0.3	1.8 ± 0.0	0.7 ± 0.0	12	3.0 ± 0.2	55	3.7 ± 0.1	67
		1.3	23.8 ± 1.7	6.5 ± 0.2	9.3 ± 0.2	39	8.1 ± 1.2	34	17.3 ± 0.3	73
		1.8	66.7 ± 0.3	38.9 ± 2.9	25.9 ± 2.2	39	2.0 ± 2.6	3	27.8 ± 1.4	42
		2.5	114.5 ± 0.8	116.2 ± 1.2	0.0 ± 0.0	0	0.0 ± 0.0	0	0.0 ± 0.0	0
		3.5	62.4 ± 1.6	60.7 ± 2.4	0.8 ± 1.1	1	0.9 ± 2.2	1	1.7 ± 0.9	3
		5.0	80.9 ± 4.8	79.7 ± 7.0	2.3 ± 1.5	3	0.0 ± 0.0	0	2.3 ± 0.7	3
		7.0	61.8 ± 0.6	57.9 ± 2.5	0.0 ± 0.0	0	3.9 ± 1.8	6	3.9 ± 0.7	6

was an increase in Fe(III) to 9.4 μ M. Below this depth, both oxidized phases of these metals were detected in similar concentrations. At Station 9, Fe(III) was below the detection limit but interestingly, we observed the highest relative abundance of Mn(III)-L_S in porewaters of the sampling campaign, with Mn(III)-L almost entirely made up of Mn (III)-L_S (i.e., $\log K_{cond} > 13.2$). Thus, Mn(III)-L was stable even when Fe (II) was present.

At the mixing and shelf stations (excluding Station 2), the subsurface maxima associated with dMn and dFe decreased with increasing distance from the coast. The highest concentrations of dMn (774.2 μM) and dFe (782.0 μM) were detected in the mixing zone at Station 4, consistent with higher organic matter content closest to land and previous coastal transect surveys of porewater trace metals (Lenstra et al., 2022; Yedema et al., 2023). Depth profiles of dMn and dFe showed that the concentrations of both metals were lowest at shallow sediment depths, where porewaters were still oxygenated and NO_3^- was detectable. At the subsurface maxima, both dissolved oxygen and NO_3^- were nondetectable, while NH_4^+ was being produced (Fig. 4, Fig. S3). Beyond this depth horizon, dMn and dFe decreased at all oceanic stations. The concentration of dFe was similar to dMn at all depths at both mixing sites and

the shelf site closest to shore (Station 3). Conversely, at Station 1, which sits on the shelf adjacent to the Mississippi Canyon, we observed [dMn] >> [dFe] in all porewaters. We detected Mn(III)-L and Fe(III) in oxic and suboxic sediment zones at all sampling locations.

In shelf sediments, organically-complexed Mn and Fe were typically much more abundant in the oxygenated porewaters, making up to 80 and 100 % of the total dissolved pool at specific depths, respectively. Additionally, the contribution of Mn(III)-L and Fe(III) to the total dissolved pool was typically lowest in the sediment layers containing the subsurface maxima for each metal (on average 13 and 29 %, respectively; n=6). Beyond this depth horizon, we observed that Mn(III)-L and Fe(III) were present, albeit in variable abundances, comprising 0–100 % of the total dissolved pool at discrete depths.

Both strong and weak ligands contributed to the Mn(III)-L signal in porewater samples. The derived $\log K_{cond}$ of weak complexes measured in this system ranged from 11.9 to 13.2. In the river sediments at Station 9, only Mn(III)-L_S was detected below the oxygen penetration depth, while both classes were found at all depths at Station 5. At three of four mixing and shelf stations (excluding Station 3), Mn(III)-L was up to 100 % dMn at some depths and was composed of both ligand classes with

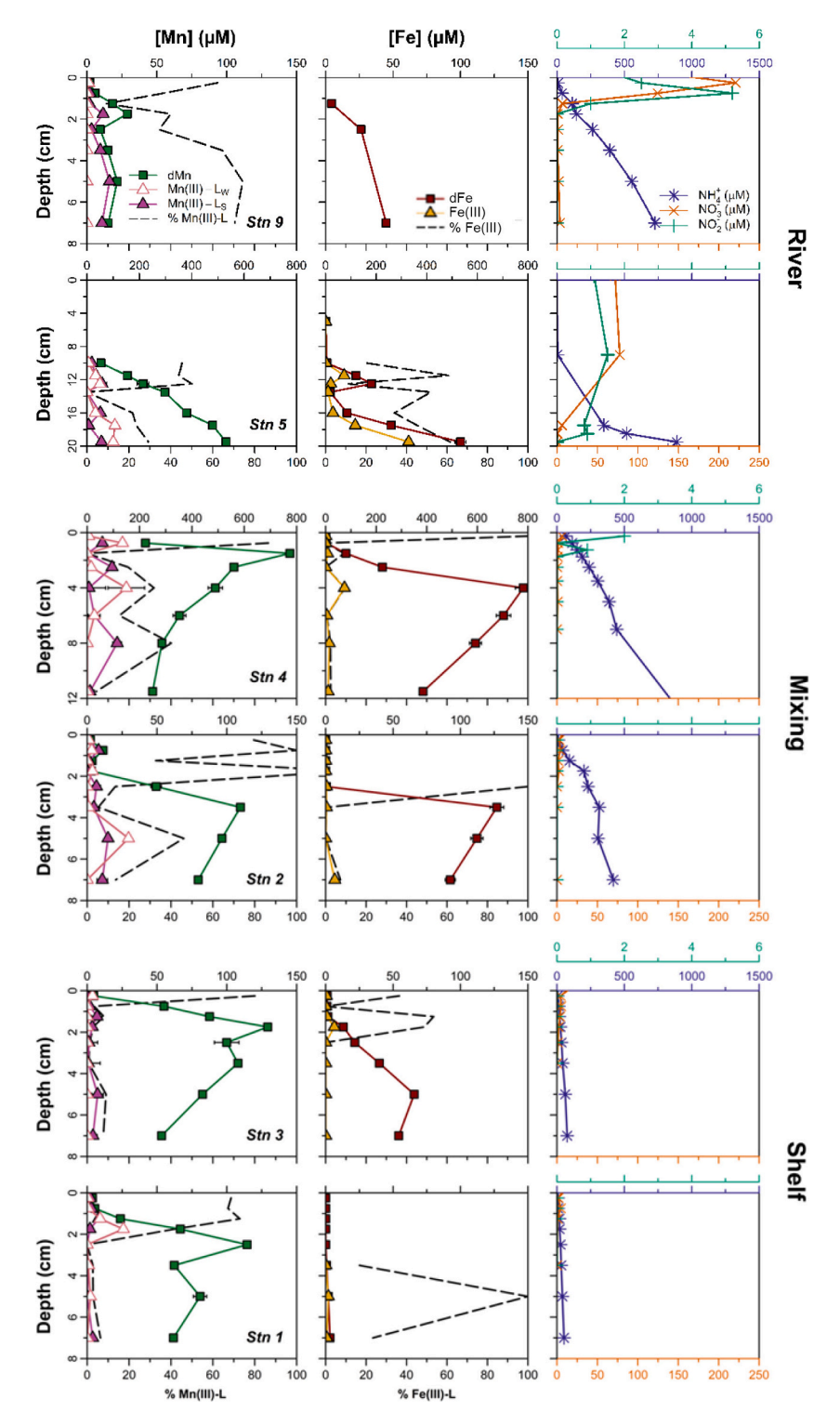


Fig. 4. Speciated porewater depth profiles of dissolved Mn (first column), dissolved Fe (second column) and N (third column). For N profiles, N species are color coded; line colors correspond to the matching color axis. Note the scale change for Mn and Fe at Stations 5 and 9. (For interpretation of the references to color in this figure legend, the reader is referred to the web version of this article.)

strong complexes comprising up to 73 % of dMn at some depths. This trend did not hold for Station 3, which was our deepest location and displayed the lowest overall relative abundance of complexed Mn. When Mn(III)-L was detected, it was present as a strong complex below the oxygen penetration depth. Nonetheless, we detected weak Mn complexes below the oxygen penetration depth and in excess of Fe(II). Below

the oxygen penetration depth at the shelf stations, we observed that when Mn(III)- L_S was in excess of Mn(III)- L_W , there wa typically a decrease in the abundance of Fe(III). At Station 9, where Mn(III)- L_S was in excess of Mn(III)- L_W at all sediment depths, Fe(III) was non-detectable.

4. Discussion

4.1. Trace metal dynamics in the northern Gulf of Mexico

This study adds to the growing body of literature that has investigated trace metal dynamics in the Mississippi River, NGoM, and during mixing of these two endmembers (Corbett et al., 2004; Justić et al., 2022; Mellett and Buck, 2020; Owings et al., 2021; Reide Corbett et al., 2006; Shiller, 1997; Shiller and Boyle, 1991; Shim et al., 2012a; Stolpe et al., 2010; Trefry and Presley, 1982; Wade et al., 2008; Wen et al., 1999b, Wen et al., 1999a, Wen et al., 2011). However, none of these previous studies have simultaneously considered the presence of organically-bound Mn(III) in both the water column and sediment porewaters. In this work, we found that our data supports previous studies of Mn cycling in the region, but highlights how different chemical forms of Mn are dominant along the river to seawater continuum.

In this active estuarine mixing environment, we expected that many chemical species of Mn coexist and rapidly cycle. In the following sections, we discuss the various chemical processes contributing to these transformations in each hydrographic regime, focusing on sources, sinks and internal cycling with an emphasis on improving our understanding of the distributions and role of Mn(III)-L. This study improves our understanding of the Mn cycle in this dynamic region through the addition of Mn(III)-L data. Mn(II) oxidized to the particulate phase most often passes through the Mn(III) oxidation state, and similarly, reduction of MnO_x most often passes through the Mn(III) oxidation state prior to forming Mn(II) (Luther, 2005; Luther et al., 2018; Morgan, 2005). In the following sections we outline evidence from each regime that supports the inclusion of Mn(III)-L in our current understanding of the Mn cycle.

4.2. Manganese cycling in the Mississippi River

In the Mississippi River plume, Mn displayed nonconservative behavior upon mixing of Mississippi River and NGoM endmembers (Fig. S1), similar to previous studies (Shim et al., 2012b). Concentrations of dMn in the Mississippi River were primarily in the form of Mn(II) with lower concentrations of particulate MnO_x (Fig. 2). Concentrations of dMn (64.5-182.6 nM) measured in this study are similar to dMn concentrations previously reported in the lower Mississippi River during the spring (Shiller, 1997; Stolpe et al., 2010; Trefry, 1977). Downstream the concentration of dMn generally increased, especially in the surface (Fig. 2). Previous studies showed that particulate Mn (pMn) was highest in the northern portion of the river, with dMn inversely correlated with MnO_x (Shiller, 1997; Shiller and Boyle, 1991). We observed a different trend here, with the concentration of MnO_x being similar both upstream and downstream, and no inverse correlation between the two pools of Mn and particle concentration (Fig. S2). The previous observations were interpreted as being due to a pMn source from weathering, followed by reductive dissolution of the pMn along the river continuum, resulting in progressively higher concentrations of dMn. Importantly, it should be noted that pMn from these previous studies are not comparable measurements to the MnOx reported here. MnOx is a measurement of the oxidative equivalence of Mn retained on a 0.2 µm filter, while pMn includes MnO_x and adsorbed/mixed-valence Mn particles retained on the same filter. While our distributions of MnOx are slightly different than those previously reported, similar processes may be responsible for the increases in the concentration of dMn downstream. However, our observations of Mn speciation indicate that additional internal cycling processes that contribute to the distributions of dissolved and pMn.

The speciation of Mn also changed along the riverine transect. We observed a decrease in the concentration of Mn(III)-L_S downstream, and Mn(II) increased while MnO_x remained relatively constant along the same transect. These MnO_x particles are likely initially produced authigenically via microbial oxidation and are rapidly cycled between the dissolved and particulate phases during advective transport, supporting in part the idea that MnO_x reduction may support the increases

in Mn(II). However, the decrease in Mn(III)-L_S complexes is puzzling because we had hypothesized that the high organic matter content of the river would contribute to a greater stabilization of Mn(III) as Mn(III)-Ls. The role of Mn(III)-L_S as a transient redox species might explain this. Organic matter and sunlight can facilitate the reduction of MnOx, which may form Mn(III)-L in the presence of Mn(III) complexing ligands, or rapidly disproportionate to Mn(II) and/or Mn(IV) in the absence of Mn (III)-L complexing ligands. Additionally, there are thermodynamic and kinetic constraints on the abiotic oxidation of Mn(II) to Mn(III) with O2 (Luther, 2005). Any abiotic Mn oxidation occurring in the river system could be the result of preferential oxidation of Mn(III) to Mn(IV), which could explain the low concentrations of Mn(III)-L_S. Mn oxidation occurs more rapidly due to biological oxidation (Shiller and Stephens, 2005; Tebo et al., 2004; Tebo, 2019). MnO_x could be photo-reduced in surface waters and as it advects downriver, which then adds to the Mn(II) pool. Mn(III) is known to complex with the same ligands as Fe(III) (Luther et al., 2015), so another explanation for the lack of Mn(III)-L could be competition between Mn(III) and Fe(III) for the organic ligand pool. Other less likely possibilities include scavenging of Mn(III)-L onto MnO_x surfaces and its deposition to the sediments, or because Mn-oxidizing microorganisms preferentially use Mn(III)-L as an electron donor (Stumm and Morgan, 1996; Webb et al., 2005), Mn(III)-Ls is preferentially oxidized to MnOx. In both of these scenarios, however, we would expect dMn to decrease with increasing salinity, which we did not observe. Finally, the colloidal phase (>10 kD - 0.2 μm) of dMn in the water column makes up only a small portion of dMn (Joung and Shiller, 2016; Stolpe et al., 2010). When present, this colloidal fraction has been suggested to be associated with fluvic colloids, CDOM-rich colloids, and benthic remobilization followed by slow reoxidation (Shiller, 1997; Shiller and Boyle, 1991; Stolpe et al., 2010), so colloidal aggregation of Mn(III)-L is another possibility. While we are not able to distinguish between these three scenarios with our current dataset, it seems most likely that the lifetime of Mn(III)-L might be short in the Mississippi River

In addition to thermodynamic considerations, the low Mn(III)-L_S observed could be due to the analytical procedure used to quantify Mn (III)-Ls. The modified procedure to detect Mn(III)-L in the nanomolar range (Section 2.2) can only quantify Mn(III)-L complexes which have a conditional stability constant of >13.2 (i.e., Mn(III)-L_S) and does not account for weaker complexes. It is possible that a large portion of Mn (III)-L in freshwater has $log K_{cond} < 13.2$ (i.e., Mn(III)-L_w). Mn has been shown to bind with 0.4–5 nm CDOM-type molecules of terrigenous origin in the Mississippi River (Stolpe et al., 2010), and these compounds are likely humic-like substances. Krachler et al. (2015) reported that land-derived humic-type Fe(III)-L complexes have $log K_{cond}$ in the range of 8-11, and known Mn(III)-L complexes have similar or slightly higher logKcond compared to analogous Fe(III)-L complexes (Luther et al., 2015). Humic-type ligands may dominate the Mn(III)-L pool in the Mississippi River and these complexes would have $\log K_{cond} < 13.2$. This idea is supported by experiments in Delaware Bay, which demonstrated that humic material outcompeted a weak Mn(III)-pyrophosphate complex but not a strong Mn(III)-desferrioxamine-B complex (Oldham et al., 2017b). This suggests that many humic-type Mn(III)-L complexes may fall within our operational definition of Mn(III)-L_W. Terrestrial organic matter makes up a large portion of total DOM during the time of our sampling campaign in the spring (Duan et al., 2007), suggesting that Mncomplexing material could be made up primarily of weaker humic-type ligands. It is possible that Mn(III)-Lhumic was present in the Mississippi River, but it was not detected by our method, and any Mn(III)-Lhumic would be reported in this study as Mn(II).

Vertical profiles of redox species in the sediments were collected, and this has not been done in the Mississippi River prior to this study to our knowledge. Trends in the porewater distributions of Mn were consistent with those in the overlying water column. For example, the subsurface maximum of dMn concentration upriver was lower than observed downriver, mimicking the trend in dMn and MnO_x in the water column.

This may reflect a higher delivery rate of MnO_x to the sediments when $[MnO_x]$ is elevated in the water column. In sediment porewaters from previous work, dMn has a sub-surface maximum associated with the depletion of dissolved oxygen (Lenstra et al., 2022; Owings et al., 2021). The concentration of this subsurface max typically decreases with increased distance from shore (Lenstra et al., 2022), which is likely reflective of the usage of settled pMn during the remineralization of organic matter (Owings et al., 2021). The dMn profiles in porewaters at both riverine stations indicate that Mn is an important component of sediment diagenesis in the Mississippi River, though different forms of Mn may be used as electron donors at each site.

4.3. Manganese cycling in the northern Gulf of Mexico

Physicochemical partitioning of Mn changed significantly relative to Mississippi River freshwater endmembers in the estuarine mixing zone (surface salinity <30, Table 1). Mn(III)-L complexes were detected at all stations and nearly all depths sampled, at times making up to 100 % of dMn (Fig. 3). This is in agreement with previous studies which observed stable Mn(III)-L complexes in oxygenated waters (Jones et al., 2020; Oldham et al., 2017b, 2020; Thibault de Chanvalon et al., 2023). Several processes can contribute to transformations of Mn and the formation and stabilization of Mn(III)-L, including physical mixing processes, internal cycling by the microbial community, and the identity and concentration of Mn(III)-binding ligands at each station. While the former two processes have been studied in some detail, the latter has not and could shed light on the residence time of Mn(III)-L in addition to the effect different ligand pools have on the oxidation rate of Mn.

At both mixing stations, the upper water column is characterized by low salinity which transitions to seawater salinity at depth (Fig. 3). Transformations of dMn in transition zones between freshwater and seawater are common features in a variety of estuarine mixing zones. The concentrations of dMn observed at mid-salinities (28-30) in this study suggest both addition and removal of dMn relative to what would be expected based on simple dilution, assuming a two endmember mixing model (Fig. S1). Fluvial suspended sediments often enter the NGoM through the deposition and resuspension of fluid muds, which facilitates the transport of river-borne materials further offshore (Corbett et al., 2004; Corbett et al., 2006). Ligand-promoted mobilization of these fluid muds could contribute to the addition of dMn to midsalinity waters here, a process which has been documented in the Broadkill River (Oldham et al., 2017a). If reductive dissolution/mobilization of MnOx is more important than direct release of Mn from the sediments, then MnO_x dissolution must be rapid to support the excess of dMn relative to MnOx observed on the shelf. The transformation of MnOx to dMn may also be due to photochemical reduction and subsequent stabilization of dMn as Mn(III)-L_S (Sunda and Huntsman, 1994). Processes contributing to the removal of dMn at mixing stations may be flocculation to suspended fluid muds transported to the NGoM from the Mississippi River, where the particles settle and are removed from solution (Maloney et al., 2020; Sholkovitz, 1978). Flocculation is likely to have an outsized effect on the removal of Mn(II) relative to Mn(III), as any Mn-stabilizing ligands would protect Mn(III)-L against coagulation (Oldham et al., 2017a). Nonetheless, because Mn(III)-L complexes in the NGoM are strong and in higher relative abundance than Mn(II), this suggests a longer residence time for Mn(III)-L in the NGoM than in the Mississippi River.

The shelf stations (1 and 3) had elevated dMn in surface waters that then decreased with depth. Shelf waters had a subsurface maximum in dMn coincident with the oxycline and enrichment of dMn in the bottom waters relative to mid-waters. Additionally, the shelf had non-detectable concentrations of MnO_x in surface waters, implicating photo-reductive dissolution of MnO_x . From 23 to 54 % of the dMn pool in the surface waters was comprised of Mn(III)-L_S, so it is likely that some portion of photo-reduced MnO_x is stabilized by ambient ligands after reduction. The high dMn in bottom waters on the shelf was predominantly in the

form of Mn(III)- L_S , likely due to a benthic diffusive flux of dMn and/or sedimentary resuspension. Our diffusive flux model (Section 4.4) indicates that there is a lower diffusive flux of Mn(III)-L than Mn(II) out of the sediments on the shelf. Because dMn was 100 % Mn(III)- L_S in bottom waters at this location, Mn(II) diffusing from sediments is likely oxidized upon escape to the water column and stabilized as Mn(III)- L_S (Table 4). It is also possible that some portion of Mn(III)- L_S in these bottom waters is comprised of colloidal MnO_X particles formed from oxidation that is accelerated due adsorption onto fluid mud material (Homoky et al., 2011). However, colloidal Mn, if present, is typically a very small portion of the overall Mn pool, even in fluid mud-rich bottom waters of the Mississippi River delta region (Joung and Shiller, 2016) and colloidal MnO_X is unstable in seawater as even trace concentrations of positively charged ions cause it to rapidly coagulate and precipitate (Jones and Tebo, 2021; Perez-Benito et al., 1989).

4.4. Mn cycling in northern Gulf of Mexico porewaters

The most striking finding from porewaters in this study was the presence of Mn(III)-L in most porewaters sampled in the NGoM. The abundant Mn(III)-L complexes which stabilize Mn(III)-L against reduction by Fe(II) in porewaters are consistent with observations reported from other estuarine systems, such as the St. Lawrence estuary (Madison et al., 2013; Oldham et al., 2019). However, they are in contrast with other porewater observations in the NGoM where Mn(III)-L was below the methodological detection limit (1 μ M; Owings et al., 2021). This difference is likely due to seasonal differences in Mn partitioning associated with late summer hypoxia sampled during that study. Owings et al. (2021) conducted their study during the summer towards the end of the hypoxic season (Rabalais et al., 2001; Rabalais and Turner, 2017). Owings et al. (2021) reported deeper subsurface dMn maxima than what we observed (Fig. 4). The shallower subsurface dMn maxima and higher Mn(III)-L observed during our spring sampling could be due to seasonal differences in productivity. Larger organic matter delivery to the sediments resulting from larger freshwater flux during the spring than the summer, coupled to shifts in the biological community as a result of hypoxia, could result in a higher chemical oxidant demand in upper sediment layers during the spring. The effects of hypoxia are both chemical and biological due to hypoxic impacts on benthic mega- and micro-faunal biodiversity (Rabalais and Baustian, 2020). The hypoxic zone during the sampling period of Owings et al. (2021) was the largest surface area since hypoxia monitoring began (Rabalais and Turner, 2017). Thus, Mn speciation reported during the summer is consistent with greater Mn(II) accumulation in sediments because of the role that MnO_x plays as an oxidant in place of O₂ for organic carbon remineralization.

There could also be methodological considerations that would explain the differences in Mn(III)-L between these two studies. In addition to measuring Mn(III)-L $_W$, we also used a final reduction step to quantify any Mn(III)-L $_S$, while Owings et al. only quantified Mn(III)-L $_W$, likely underestimated the total concentration of Mn(III)-L. Typically, we

Table 4
Calculated diffusive benthic fluxes of speciated dissolved Mn. Negative values indicate flux from the sediments to the overlying water column. The Mn(III) flux column represents the values calculated assuming ionic Mn(III) flux across the sediment water interface, while the Mn(III)-L flux column represents values calculated assuming Mn(III) bound to 0.5–1 kDa humic-like organic material across the sediment water interface.

Station	Mn(II) flux	Mn(III) flux	Mn(III)-L flux	
	μ M m^{-2} d^{-1}	μ M m^{-2} d^{-1}	$\mu M m^{-2} d^{-1}$	
4	-13.0	-6.0	-2.6	
2	-3.8	-8.2	-5.6	
3	-15.5	-13	-3.5	
1	-13.8	-25.5	-10.9	

J.E. Davis et al. Marine Chemistry 267 (2024) 104466

observed that Mn(III)- L_S was a major fraction of Mn(III)-L in the suboxic porewaters. Based on our results here and the methodology used by Owings et al. (2021), dMn reported by them likely overlooked a fraction of Mn(III)- L_S . There could also be a significant fraction of dMn in porewaters that is in the colloidal fraction, that might be detected as Mn (III)- L_S in this work, even if it is actually not organically-bound Mn (Homoky et al., 2011). The chemical speciation of colloidal Mn is unknown, and could include both inorganic and organic phases. Uncovering the speciation of colloidal Mn in porewaters will be important in future studies, to fully understand how this fraction might impact Mn transformations in sediments.

In addition to seasonal changes that impact the redox environment of these two sampling periods, seasonal hypoxia alters benthic community composition and abundance in the NGoM (Rabalais and Baustian, 2020; Shivarudrappa and Briggs, 2017). Total biomass of the most abundant macroinfaunal species significantly decreases when bottom water O_2 is depleted, and the dominant feeding modality shifts from an even mix between subsurface deposit feeders and surface deposit feeders to nearly completely surface deposit feeders (Rabalais and Baustian, 2020). This shift in feeding modality has the potential to affect bioturbation rates in the sediments, which would potentially impact the ability of Mn(II) to be oxidized to Mn(III)-L in suboxic sediments, and its diffusion into the overlying water column.

4.5. Filling in knowledge gaps about Mn(III)-L cycling in the northern Gulf of Mexico

This was the first study to thoroughly examine Mn speciation in the water column and sediment porewaters of the NGoM, particularly with respect to characterizing the cycling of Mn(III)-L. To quantify the potential importance of Mn(III)-L in the Mn cycle in the NGoM, specifically in the Mississippi River delta region, we constructed a simple mass balance box model of the NGoM that included the main sources and sinks of dMn (Fig. 5, Table S1 and S2). We assumed a steady state model, and the primary sources considered were riverine input from the Mississippi and Atchafalaya Rivers, dust deposition, and diffusive input from the sediments. The primary sinks were phytoplankton uptake of dMn, abiotic and biotic Mn oxidation, and flocculation of dMn during estuarine mixing. We calculated two versions of this model; one assumed that the only oxidation state of Mn contributing to the dissolved phase in the NGoM was Mn(II), while the other assumed that Mn(II) and Mn(III)

L both contributed to the dissolved phase of Mn (Table S1 and S2).

The fluxes in the box model were quantified based on both data from this study and others (Fig. 5). The volume of the NGoM box was determined by multiplying the surface area of the of the continental shelf between 93.8059°W and 87.5086°W (1.8 \times 10^{11} $m^2)$ by the average depth of the continental shelf (120 m) (Donoghue, 2011). The flux of dMn from the Mississippi River was calculated by multiplying the average [dMn] measured in the Mississippi River in this study by the annual average volumetric flux of both the Mississippi River in 2021 (USGS Monitoring Station 07374525, Mississippi River at Belle Chasse, Louisiana) and Atchafalaya River in 2021 (USGS Monitoring Station 07381600, Atchafalaya River at Morgan City, Louisiana). Although the concentration of dMn was not measured in the Atchafalaya River in this study, dMn in the two rivers is similar (Reiman et al., 2018). Mn inputs to the NGoM from dust deposition were approximated using the average dust flux to the region (Kok et al., 2021) and assuming a dissolution efficiency of 0.22 nM day⁻¹ mg dust⁻¹ (Mendez et al., 2010). The diffusive sedimentary flux of dMn was calculated by averaging the diffusive flux rates quantified in our Fickian flux model (Table 4) multiplied by the surface area of the continental shelf and was calculated using both the diffusion rate of ionic Mn(III) and of Mn(III) bound to 0.5–1 kDa humic acid-like organic material (Table 4). Sholkovitz (1978) reported that 25-45 % of dMn flocculates and is lost from solution during estuarine mixing. To account for this in our model, we used the median value of this range and assumed that 35 % of dMn was lost from the riverine flux of dMn into the box model area. Phytoplankton uptake was quantified using the average annual primary productivity rate in the NGoM (Benway and Coble, 2014), a mean C:chl a ratio of 60 (Bowie et al., 2001), and a mean Mn:C ratio of 3.7 μ mol Mn mol C⁻¹ (Martin and Knauer, 1973). Finally, an average microbial oxidation rate was estimated using the difference between dissolved sources and sinks to the NGoM over an annual cycle and assuming the maintenance of steady state. For additional details on the box model calculations, refer to supplementary Table S1 and S2.

Considering only Mn(II) in the source and sink terms and assuming a residence time range of 6 months to 1 year (Wang et al., 2016), the mass balance estimated that the average concentration of dMn would be on the order of 177.4–354.9 nM. On the other hand, when both Mn(II) and Mn(III)-L were considered in the source and sink terms and assuming the same residence time as above, the mass balance estimated that the background concentration of dMn in the NGoM would be between 28.4

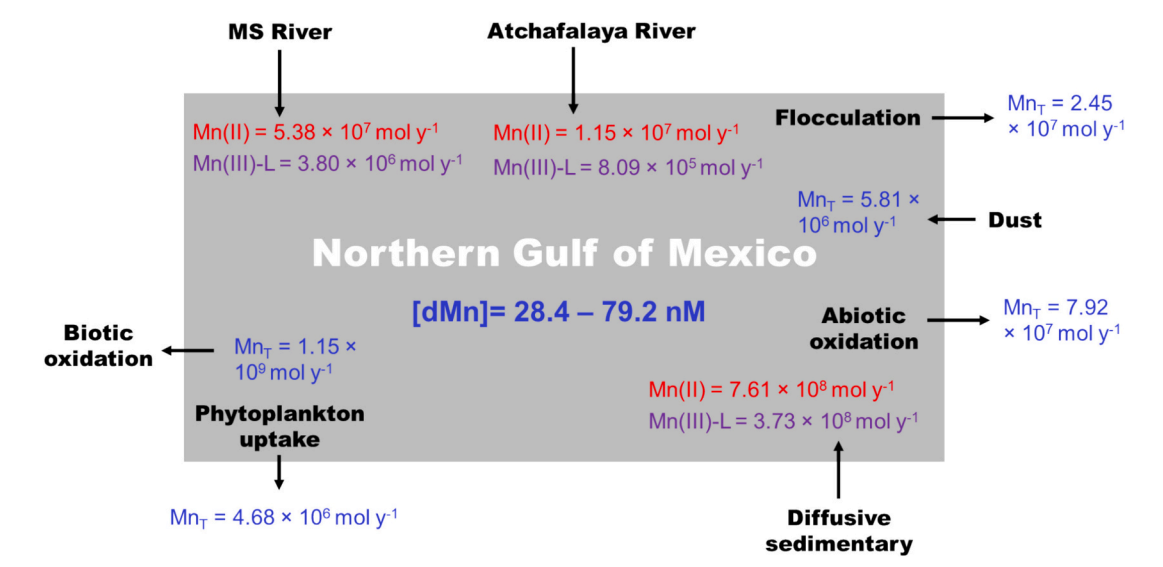


Fig. 5. Sources and sinks of dissolved Mn(II) and Mn(III)-L considered in the box model of the Northern Gulf of Mexico. Fluxes included in the figure come from the calculation incorporating Mn(III)-L diffusive sedimentary flux. Red and purple text indicates model parameters that had Mn(II) and Mn(III)-L data to incorporate into the calculations, respectively. Blue text indicates model parameters that did not have speciated dMn data to include. (For interpretation of the references to color in this figure legend, the reader is referred to the web version of this article.)

and 79.2 nM. The average concentration of dMn measured in this study in the NGoM was 43.2 \pm 40.7 nM (n=23). The box model that considered both Mn(II) and Mn(III)-L in the source and sink terms of dMn in the NGoM were much better aligned with our measurements compared to the Mn(II) only model. Although simplified, these back of the envelope calculations demonstrated that fluxes of Mn(III)-L are likely necessary to include in modelling efforts in order to better reproduce background concentrations of dMn in the NGoM, and likely in other regions of the global ocean. The presence of Mn(III)-L in coastal regions and in the open ocean more broadly, could have important implications for how we think about Mn as a scavenger of the sea.

5. Conclusions

These results demonstrate the need to recharacterize the Mn cycle in the marine environment and include fluxes of Mn(III)-L. We demonstrated that Mn(III)-L is often a dominant fraction of dMn in the water column and sediment porewaters of a highly dynamic estuarine system, implying that estuarine transformation of Mn, and thus delivery to the global ocean, is likely much more nuanced than previously described. During estuarine mixing in the NGoM, the dissolved pool of Mn shifted from largely Mn(II) in the Mississippi River to primarily Mn(III)-L when [MnO_x] < dMn. Our results suggest that the natural ligand pool could contribute to reductive partitioning of MnO_x into the dissolved phase as Mississippi River and NGoM endmembers meet, with Mn(III)-L_S stabilized by ambient organic ligands as the product. Previous mass-balanced based approaches to quantify riverine delivery of Mn to the ocean have assumed either estuarine removal or conservative mixing, yet our results indicate that these approaches could be misrepresenting riverine dMn delivery to the ocean. Additionally, we demonstrated Mn(III)-L flux from sedimentary porewaters for the first time, characterizing an overlooked source of Mn(III)-L to the water column of estuarine systems. As Mn(III)-L are thought to be ubiquitous in the marine environment, these findings have broad implications for sedimentary sources of Mn(III)-L throughout the global ocean and understanding the oxidation state of Mn from sediments is crucial for quantifying the residence time and propensity for long-range transport of dMn. Finally, the more accurate representation of the Mn cycle in the NGoM from our simple box model that included Mn(III)-L dynamics highlighted the importance of including the cycling of Mn(III)-L in our understanding of the Mn cycle in the global ocean.

CRediT authorship contribution statement

Jessalyn E. Davis: Writing – original draft, Visualization, Methodology, Investigation, Formal analysis, Data curation. Rebecca S. Robinson: Writing – review & editing, Validation, Resources, Project administration, Methodology, Investigation, Funding acquisition, Data curation, Conceptualization. Emily R. Estes: Writing – review & editing, Project administration, Methodology, Investigation, Funding acquisition, Conceptualization. Veronique E. Oldham: Writing – review & editing, Project administration, Methodology, Investigation, Funding acquisition, Data curation, Conceptualization. Evan A. Solomon: Writing – review & editing, Supervision, Methodology. Roger P. Kelly: Writing – review & editing, Validation, Resources, Project administration, Investigation. Katherine E. Bell: Investigation, Software. Joseph A. Resing: Writing – review & editing, Supervision, Methodology. Randelle M. Bundy: Writing – review & editing, Supervision, Methodology.

Data availability

Supporting data from this publication can be found at https://doi.org/10.5281/zenodo.10895395.

Acknowledgements

We would like to thank the captain and crew of the R/V *Pelican*. We also would like to thank Ryan McGinnis for conducting MnO_x analyses along with James Murray and two anonymous reviewers for helpful comments on this manuscript. This work was funded by the National Science Foundation (OCE-2022782), the National Science Foundation Graduate Research Fellowship Program (DGE-2140004), and the Cooperative Institute for Climate, Ocean, and Ecosystem Studies Graduate Fellowship (2024-1395), with support from the Pacific Marine Environmental Laboratory (5670).

Appendix A. Supplementary data

Supplementary data to this article can be found online at https://doi.org/10.1016/j.marchem.2024.104466.

References

- Allison, M.A., Bianchi, T.S., McKee, B.A., Sampere, T.P., 2007. Carbon burial on river-dominated continental shelves: impact of historical changes in sediment loading adjacent to the Mississippi River. Geophys. Res. Lett. 34. https://doi.org/10.1029/2006GI.028362.
- Altmann, H.J., 1972. Bestimmung von in Wasser gelöstem Sauerstoff mit Leukoberbelinblau I. Fresenius Z. Für Anal. Chem. 262, 97–99. https://doi.org/ 10.1007/BF00425919.
- Barnes, H., 1984. Oceanography and Marine Biology, an Annual Review, 22. CRC Press. Benway, H.M., Coble, P.G., 2014. Report of the Gulf of Mexico Coastal Carbon Synthesis Workshop.
- Berg, R.D., Solomon, E.A., Teng, F.-Z., 2019. The role of marine sediment diagenesis in the modern oceanic magnesium cycle. Nat. Commun. 10, 4371. https://doi.org/ 10.1038/s41467-019-12322-2
- Bianchi, T.S., Mitra, S., McKee, B.A., 2002. Sources of terrestrially-derived organic carbon in lower Mississippi River and Louisiana shelf sediments: implications for differential sedimentation and transport at the coastal margin. Mar. Chem. 77, 211–223. https://doi.org/10.1016/S0304-4203(01)00088-3.
- Boudreau, B.P., 1997. Diagenetic Models and their Implementation: Modelling Transport and Reactions in Aquatic Sediments. Springer.
- Bowie, A.R., Maldonado, M.T., Frew, R.D., Croot, P.L., Achterberg, E.P., Mantoura, R. Fauzi C., Worsfold, P.J., Law, C.S., Boyd, P.W. 2001. The fate of added iron during a mesoscale fertilisation experiment in the Southern Ocean. Deep Sea Res. 2 Top. Stud. Oceanogr. 48. pp. 2703-2743. doi: 10.1016/S0967-0645(01)00015-7.
- Boyle, E., Collier, R., Dengler, A.T., Edmond, J.M., Ng, A.C., Stallard, R.F., 1974. On the chemical mass-balance in estuaries. Geochim. Cosmochim. Acta 38, 1719–1728. https://doi.org/10.1016/0016-7037(74)90188-4.
- Boyle, E.A., Edmond, J.M., Sholkovitz, E.R., 1977. The mechanism of iron removal in estuaries. Geochim. Cosmochim. Acta 41, 1313–1324. https://doi.org/10.1016/ 0016-7037(77)90075-8.
- Buck, K.N., Sohst, B., Sedwick, P.N., 2015. The organic complexation of dissolved iron along the U.S. GEOTRACES (GA03) North Atlantic section. In: Deep Sea Res. Part II Top. Stud. Oceanogr., GEOTRACES GA-03 - the U.S. Geotraces North Atlantic Transect, 116, pp. 152–165. https://doi.org/10.1016/j.dsr2.2014.11.016.
- Canfield, D.E., Kristensen, Erik, Thamdrup, Bo, 2005. The Iron and manganese cycles. In:
 Canfield, D.E., Kristensen, E., Thamdrup, B. (Eds.), Advances in Marine Biology,
 Aquatic Geomicrobiology. Academic Press, pp. 269–312. https://doi.org/10.1016/ S0065-2881(05)48008-6.
- Corbett, D.R., McKee, B., Duncan, D., 2004. An evaluation of mobile mud dynamics in the Mississippi River deltaic region. Mar. Geol. 209, 91–112. https://doi.org/ 10.1016/j.margeo.2004.05.028.
- Corbett, D.R., McKee, B., Allison, M., 2006. Nature of decadal-scale sediment accumulation on the western shelf of the Mississippi River delta. In: Cont. Shelf Res., Special Issue in Honor of Richard W. Sternberg's Contributions to Marine Sedimentology, 26, pp. 2125–2140. https://doi.org/10.1016/j.csr.2006.07.012.
- Cornel, P.K., Summers, R.S., Roberts, P.V., 1986. Diffusion of humic acid in dilute aqueous solution. J. Colloid Interface Sci. 110, 149–164. https://doi.org/10.1016/ 0021-9797(86)90364-4.
- Donoghue, J.F., 2011. Sea level history of the northern Gulf of Mexico coast and sea level rise scenarios for the near future. Clim. Chang. 107, 17–33. https://doi.org/
- Duan, S., Bianchi, T.S., Sampere, T.P., 2007. Temporal variability in the composition and abundance of terrestrially-derived dissolved organic matter in the lower Mississippi and pearl Rivers. Mar. Chem. 103, 172–184. https://doi.org/10.1016/j. marchem.2006.07.003.
- Froelich, P.N., Klinkhammer, G.P., Bender, M.L., Luedtke, N.A., Heath, G.R., Cullen, D., Dauphin, P., Hammond, D., Hartman, B., Maynard, V., 1979. Early oxidation of organic matter in pelagic sediments of the eastern equatorial Atlantic: suboxic diagenesis. Geochim. Cosmochim. Acta 43, 1075–1090. https://doi.org/10.1016/0016-7037(79)90095-4.

Marine Chemistry 267 (2024) 104466

- Gledhill, M., Buck, K., 2012. The organic complexation of Iron in the marine environment: a review. Front. Microbiol. 3. https://doi.org/10.3389/ fmicb.2012.00069.
- Goldberg, E.D., 1954. Marine geochemistry 1. Chemical scavengers of the sea. J. Geol. 62, 249–265.
- Hansel, C.M., 2017. Chapter two manganese in marine microbiology. In: Poole, R.K. (Ed.), Advances in Microbial Physiology, Microbiology of Metal Ions. Academic Press, pp. 37–83. https://doi.org/10.1016/bs.ampbs.2017.01.005.
- Hedges, J.I., Keil, R.G., 1999. Organic geochemical perspectives on estuarine processes: sorption reactions and consequences. Mar. Chem. 65, 55–65. https://doi.org/ 10.1016/S0304-4203(99)00010-9.
- Holmes, R.M., Aminot, A. Kérouel, R. Hooker, B.A., Peterson, B.J. 1999. A simple and precise method for measuring ammonium in marine and freshwater ecosystems. Can. J. Fish. Aquat. Sci. 56. pp. 1801-1808. doi:10.1139/f99-128.
- Homoky, W.B., Hembury, D.J., Hepburn, L.E., Mills, R.A., Statham, P.J., Fones, G.R., Palmer, M.R., 2011. Iron and manganese diagenesis in deep sea volcanogenic sediments and the origins of pore water colloids. Geochim. Cosmochim. Acta 75, 5032–5048. https://doi.org/10.1016/j.gca.2011.06.019.
- Javanaud, C., Michotey, V., Guasco, S., Garcia, N., Anschutz, P., Canton, M., Bonin, P., 2011. Anaerobic ammonium oxidation mediated by Mn-oxides: from sediment to strain level. Res. Microbiol. 162, 848–857. https://doi.org/10.1016/j. resmic.2011.011.
- Jones, M.R., Tebo, B.M., 2021. Novel manganese cycling at very low ionic strengths in the Columbia River estuary. Water Res. 207, 117801. https://doi.org/10.1016/j. watres 2021 117801
- Jones, M.E., Beckler, J.S., Taillefert, M., 2011. The flux of soluble organic-iron(III) complexes from sediments represents a source of stable iron(III) to estuarine waters and to the continental shelf. Limnol. Oceanogr. 56, 1811–1823. https://doi.org/10.4319/lo.2011.56.5.1811.
- Jones, M.R., Oldham, V.E., Luther, G.W., Mucci, A., Tebo, B.M., 2019. Distribution of desferrioxamine-B-extractable soluble manganese(III) and particulate MnO2 in the St. Lawrence estuary, Canada. Mar. Chem. 208, 70–82. https://doi.org/10.1016/j. marchem.2018.11.005.
- Jones, M.R., Luther, G.W., Tebo, B.M., 2020. Distribution and concentration of soluble manganese(II), soluble reactive Mn(III)-L, and particulate MnO2 in the Northwest Atlantic Ocean. Mar. Chem. 226, 103858. https://doi.org/10.1016/j. marchem.2020.103858.
- Joung, D., Shiller, A.M., 2016. Temporal and spatial variations of dissolved and colloidal trace elements in Louisiana shelf waters. Mar. Chem. 181, 25–43. https://doi.org/ 10.1016/j.marchem.2016.03.003.
- Justić, D., Kourafalou, V., Mariotti, G., He, S., Weisberg, R., Androulidakis, Y., Barker, C., Bracco, A., Dzwonkowski, B., Hu, C., Huang, H., Jacobs, G., Le Hénaff, M., Liu, Y., Morey, S., Nittrouer, J., Overton, E., Paris, C.B., Roberts, B.J., Rose, K., Valle-Levinson, A., Wiggert, J., 2022. Transport processes in the Gulf of Mexico along the river-estuary-Shelf-Ocean continuum: a review of research from the Gulf of Mexico research initiative. Estuar. Coasts 45, 621–657. https://doi.org/10.1007/s12237-021-01005-1.
- Kok, J.F., Adebiyi, A.A., Albani, S., Balkanski, Y., Checa-Garcia, R., Chin, M., Colarco, P. R., Hamilton, D.S., Huang, Y., Ito, A., Klose, M., Leung, D.M., Li, L., Mahowald, N.M., Miller, R.L., Obiso, V., Pérez García-Pando, C., Rocha-Lima, A., Wan, J.S., Whicker, C.A., 2021. Improved representation of the global dust cycle using observational constraints on dust properties and abundance. Atmos. Chem. Phys. 21, 8127–8167. https://doi.org/10.5194/acp-21-8127-2021.
- Kostka, J.E., Luther, G.W., Nealson, K.H., 1995. Chemical and biological reduction of Mn (III)-pyrophosphate complexes: potential importance of dissolved Mn (III) as an environmental oxidant. Geochim. Cosmochim. Acta 59, 885–894. https://doi.org/ 10.1016/0016-7037(95)00007-0.
- Krachler, R., Krachler, R.F., Wallner, G., Hann, S., Laux, M., Cervantes Recalde, M.F., Jirsa, F., Neubauer, E., von der Kammer, F., Hofmann, T., Keppler, B.K., 2015. Riverderived humic substances as iron chelators in seawater. Mar. Chem. 174, 85–93. https://doi.org/10.1016/j.marchem.2015.05.009.
- Lenstra, W.K., van Helmond, N.A.G.M., Żygadłowska, O.M., van Zummeren, R., Witbaard, R., Slomp, C.P., 2022. Sediments as a source of Iron, manganese, cobalt and nickel to continental shelf waters (Louisiana, Gulf of Mexico). Front. Mar. Sci. 9. https://doi.org/10.3389/fmars.2022.811953.
- Lin, H., Taillefert, M., 2014. Key geochemical factors regulating Mn(IV)-catalyzed anaerobic nitrification in coastal marine sediments. Geochim. Cosmochim. Acta 133, 17–33. https://doi.org/10.1016/j.gca.2014.01.025.
- Luther, G.W., 2005. Manganese(II) oxidation and Mn(IV) reduction in the environment—two one-Electron transfer steps versus a single two-Electron step. Geomicrobiol J. 22, 195–203. https://doi.org/10.1080/01490450590946022.
- Luther, G.W., Sundby, B., Lewis, B.L., Brendel, P.J., Silverberg, N., 1997. Interactions of manganese with the nitrogen cycle: alternative pathways to dinitrogen. Geochim. Cosmochim. Acta 61, 4043–4052. https://doi.org/10.1016/S0016-7037(97)00239-1.
- Luther, G.W., Madison, A.S., Mucci, A., Sundby, B., Oldham, V.E., 2015. A kinetic approach to assess the strengths of ligands bound to soluble Mn(III). In: Mar. Chem., SCOR WG 139: organic ligands A Key Control on trace Metal Biogeochemistry in the Ocean, 173, pp. 93–99. https://doi.org/10.1016/j.marchem.2014.09.006.
- Luther, G.W., Thibault de Chanvalon, A., Oldham, V.E., Estes, E.R., Tebo, B.M., Madison, A.S., 2018. Reduction of manganese oxides: thermodynamic, kinetic and mechanistic considerations for one- versus two-Electron transfer steps. Aquat. Geochem. 24, 257–277. https://doi.org/10.1007/s10498-018-9342-1.
- Madison, A.S., Tebo, B.M., Luther, G.W., 2011. Simultaneous determination of soluble manganese(III), manganese(II) and total manganese in natural (pore)waters. Talanta 84, 374–381. https://doi.org/10.1016/j.talanta.2011.01.025.

- Madison, A.S., Tebo, B.M., Mucci, A., Sundby, B., Luther, G.W., 2013. Abundant Porewater Mn(III) Is a Major Component of the Sedimentary Redox System. Sci 341, 875–878. https://doi.org/10.1126/science.1241396.
- Malcolm, R.L., Durum, W.H., 1976. Organic carbon and nitrogen concentrations and annual organic carbon load of six selected rivers of the United States (USGS numbered series no. 1817- F), organic carbon and nitrogen concentrations and annual organic carbon load of six selected rivers of the United States. In: Water Supply Paper. For Sale by the Supt. of Docs., U.S. Govt. Print. Off. https://doi.org/ 10.3133/wsp1817F.
- Maloney, J.M., Bentley, S.J., Xu, K., Obelcz, J., Georgiou, I.Y., Jafari, N.H., Miner, M.D., 2020. Mass wasting on the Mississippi River subaqueous delta. Earth Sci. Rev. 200, 103001. https://doi.org/10.1016/j.earscirev.2019.103001.
- Martin, J.H., Knauer, G.A., 1973. The elemental composition of plankton. Geochim. Cosmochim. Acta 37, 1639–1653. https://doi.org/10.1016/0016-7037(73)90154-3.
- Mellett, T., Buck, K.N., 2020. Spatial and temporal variability of trace metals (Fe, Cu, Mn, Zn, Co, Ni, Cd, Pb), iron and copper speciation, and electroactive Fe-binding humic substances in surface waters of the eastern Gulf of Mexico. Mar. Chem. 227, 103891. https://doi.org/10.1016/j.marchem.2020.103891.
- Mendez, J., Guieu, C., Adkins, J., 2010. Atmospheric input of manganese and iron to the ocean: seawater dissolution experiments with Saharan and north American dusts. In: Mar. Chem., Aerosol Chemistry and Impacts on the Ocean, 120, pp. 34–43. https:// doi.org/10.1016/j.marchem.2008.08.006.
- Moore, R.M., Burton, J.D., Williams, P.J.LeB, Young, M.L., 1979. The behaviour of dissolved organic material, iron and manganese in estuarine mixing. Geochim. Cosmochim. Acta 43, 919–926. https://doi.org/10.1016/0016-7037(79)90229-1
- Moore, L.E., Heller, M.I., Barbeau, K.A., Moffett, J.W., Bundy, R.M., 2021. Organic complexation of iron by strong ligands and siderophores in the eastern tropical North Pacific oxygen deficient zone. Mar. Chem. 236, 104021. https://doi.org/ 10.1016/j.marchem.2021.104021.
- Morgan, J.J., 2005. Kinetics of reaction between O2 and Mn(II) species in aqueous solutions. Geochim. Cosmochim. Acta 69, 35–48. https://doi.org/10.1016/j. gca.2004.06.013.
- Oldham, V.E., Owings, S.M., Jones, M.R., Tebo, B.M., Luther, G.W., 2015. Evidence for the presence of strong Mn(III)-binding ligands in the water column of the Chesapeake Bay. Mar. Chem. 171, 58–66. https://doi.org/10.1016/j. marchem.2015.02.008.
- Oldham, V.E., Jones, M.R., Tebo, B.M., Luther, G.W., 2017a. Oxidative and reductive processes contributing to manganese cycling at oxic-anoxic interfaces. In: Mar. Chem., SI: Honoring Frank Millero, 195, pp. 122–128. https://doi.org/10.1016/j. marchem.2017.06.002.
- Oldham, V.E., Miller, M.T., Jensen, L.T., Luther, G.W., 2017b. Revisiting Mn and Fe removal in humic rich estuaries. Geochim. Cosmochim. Acta 209, 267–283. https://doi.org/10.1016/j.gca.2017.04.001.
- Oldham, V.E., Mucci, A., Tebo, B.M., Luther, G.W., 2017c. Soluble Mn(III)—L complexes are abundant in oxygenated waters and stabilized by humic ligands. Geochim. Cosmochim. Acta 199, 238–246. https://doi.org/10.1016/j.gca.2016.11.043.
- Oldham, V.E., Siebecker, M.G., Jones, M.R., Mucci, A., Tebo, B.M., Luther, G.W., 2019. The speciation and mobility of Mn and Fe in estuarine sediments. Aquat. Geochem. 25, 3–26. https://doi.org/10.1007/s10498-019-09351-0.
- Oldham, V.E., Lamborg, C.H., Hansel, C.M., 2020. The Spatial and Temporal Variability of Mn Speciation in the Coastal Northwest Atlantic Ocean. J. Geophys. Res. Oceans 125, e2019JC015167. https://doi.org/10.1029/2019JC015167.
- Oldham, V.E., Chmiel, R., Hansel, C.M., DiTullio, G.R., Rao, D., Saito, M., 2021. Inhibited manganese oxide formation hinders cobalt scavenging in the Ross Sea. Glob. Biogeochem. Cycles 35, e2020GB006706. https://doi.org/10.1029/2020GB006706.
- Owings, S.M., Bréthous, L., Eitel, E.M., Fields, B.P., Boever, A., Beckler, J.S., Bombled, B., Lansard, B., Metzger, E., Rabouille, C., Taillefert, M., 2021. Differential manganese and iron recycling and transport in continental margin sediments of the northern Gulf of Mexico. Mar. Chem. 229, 103908. https://doi.org/10.1016/j. marchem.2020.103908.
- Parker, D.L., Morita, T., Mozafarzadeh, M.L., Verity, R., McCarthy, J.K., Tebo, B.M., 2007. Inter-relationships of MnO2 precipitation, siderophore—Mn(III) complex formation, siderophore degradation, and iron limitation in Mn(II)-oxidizing bacterial cultures. In: Geochim. Cosmochim. Acta, Physical Chemistry of Soils and Aquifers: A Special Issue in Honor of Garrison Sposito, 71, pp. 5672–5683. https://doi.org/10.1016/j.gca.2007.03.042.
- Perez-Benito, J.F., Brillas, E., Pouplana, R., 1989. Identification of a soluble form of colloidal manganese(IV). Inorg. Chem. 28, 390–392. https://doi.org/10.1021/ ic00302a002.
- Rabalais, N.N., Baustian, M.M., 2020. Historical shifts in benthic Infaunal diversity in the northern Gulf of Mexico since the appearance of seasonally severe hypoxia. Diversity 12, 49. https://doi.org/10.3390/d12020049.
- Rabalais, N.N., Turner, R.E., 2017. Summary of 2017 Research Cruise Press Release (Gulf of Mexico).
- Rabalais, N.N., Turner, R.E., Wiseman Jr., W.J., 2001. Hypoxia in the Gulf of Mexico. J. Environ. Qual. 30, 320–329. https://doi.org/10.2134/jeq2001.302320x.
- Reiman, J.H., Xu, Y.J., He, S., DelDuco, E.M., 2018. Metals geochemistry and mass export from the Mississippi-Atchafalaya River system to the northern Gulf of Mexico. Chemosphere 205, 559–569. https://doi.org/10.1016/j.chemosphere.2018.04.094.
- Shiller, A.M., 1997. Dissolved trace elements in the Mississippi River: seasonal, interannual, and decadal variability. Geochim. Cosmochim. Acta 61, 4321–4330. https://doi.org/10.1016/S0016-7037(97)00245-7.
- Shiller, A.M., Boyle, E.A., 1991. Trace elements in the Mississippi River Delta outflow region: behavior at high discharge. In: Geochim. Cosmochim. Acta, The Macalpine Hills Lunar Meteorite Consortium, 55, pp. 3241–3251. https://doi.org/10.1016/ 0016-7037(91)90486-0.

- Shiller, A.M., Stephens, T.H., 2005. Microbial manganese oxidation in the lower Mississippi River: methods and evidence. Geomicrobiol J. 22, 117–125. https://doi. org/10.1080/01490450590945924.
- Shim, M.-J., Swarzenski, P.W., Shiller, A.M., 2012a. Dissolved and colloidal trace elements in the Mississippi River delta outflow after hurricanes Katrina and Rita. Cont. Shelf Res. 42, 1–9. https://doi.org/10.1016/j.csr.2012.03.007.
- Shim, M.-J., Swarzenski, P.W., Shiller, A.M., 2012b. Dissolved and colloidal trace elements in the Mississippi River delta outflow after hurricanes Katrina and Rita. Cont. Shelf Res. 42, 1–9. https://doi.org/10.1016/j.csr.2012.03.007.
- Shivarudrappa, S.K., Briggs, K.B., 2017. Macrobenthos community succession in the northern Gulf of Mexico hypoxic regions: testing the Pearson-Rosenberg model. J. Mar. Res. 75, 18–46. https://doi.org/10.1357/002224017821219036.
- Sholkovitz, E.R., 1976. Flocculation of dissolved organic and inorganic matter during the mixing of river water and seawater. Geochim. Cosmochim. Acta 40, 831–845. https://doi.org/10.1016/0016-7037(76)90035-1.
- Sholkovitz, E.R., 1978. The flocculation of dissolved Fe, Mn, Al, cu, Ni, co and cd during estuarine mixing. Earth Planet. Sci. Lett. 41, 77–86. https://doi.org/10.1016/0012-821X(78)90043-2.
- Stolpe, B., Guo, L., Shiller, A.M., Hassellöv, M., 2010. Size and composition of colloidal organic matter and trace elements in the Mississippi River, Pearl River and the northern Gulf of Mexico, as characterized by flow field-flow fractionation. Mar. Chem. 118, 119–128. https://doi.org/10.1016/j.marchem.2009.11.007.
- Stookey, L.L., 1970. Ferrozine—a new spectrophotometric reagent for iron. Anal. Chem. 42, 779–781. https://doi.org/10.1021/ac60289a016.
- Stumm, W., Morgan, J.J., 1996. Aquatic Chemistry: Chemical Equilibria and Rates in Natural Waters. Wiley.
- Sunda, W.G., Huntsman, S.A., 1994. Photoreduction of manganese oxides in seawater. In: Mar. Chem., 12th International Symposium @'Chemistry of the Mediterranean@', 46, pp. 133–152. https://doi.org/10.1016/0304-4203(94)90051-5.
- Tebo, B.M.L., 2019. Manganese Cycling in the Oceans. In: Encycl. Water Sci. Technol. Soc. https://doi.org/10.1002/9781119300762.wsts0065.
- Tebo, B.M., Bargar, J.R., Clement, B.G., Dick, G.J., Murray, K.J., Parker, D., Verity, R., Webb, S.M., 2004. Biogenic manganese oxides: properties and mechanisms of formation. Annu. Rev. Earth Planet. Sci. 32, 287–328. https://doi.org/10.1146/annurev.earth.32.101802.120213.
- Thibault de Chanvalon, A., Luther, G.W., 2019. Mn speciation at nanomolar concentrations with a porphyrin competitive ligand and UV–vis measurements. Talanta 200, 15–21. https://doi.org/10.1016/j.talanta.2019.02.069.
- Thibault de Chanvalon, A., Luther, G.W., Estes, E.R., Necker, J., Tebo, B.M., Su, J., Cai, W.-J., 2022. Influences of iron and manganese cycling on alkalinity in the redox stratified water column of Chesapeake Bay. EGUsphere 1–23. https://doi.org/10.5194/egusphere-2022-428.
- Thibault de Chanvalon, A., Luther III, G.W., Oldham, V.E., Tebo, B.M., Coffey, N.R., Shaw, T.F., 2023. Distribution and stability of Mn complexes in the ocean: influence of hydrothermal plumes and weather events. Limnol. Oceanogr. 68, 455–466. https://doi.org/10.1002/lno.12285.
- Trefry, J.H., 1977. The Transport of Heavy Metals by the Mississippi River and their Fate in the Gulf of Mexico (Thesis).
- Trefry, J.H., Presley, B.J., 1982. Manganese fluxes from Mississippi Delta sediments. Geochim. Cosmochim. Acta 46, 1715–1726. https://doi.org/10.1016/0016-7037 (82)90112-0.
- Trouwborst, R.E., Clement, B.G., Tebo, B.M., Glazer, B.T., Luther, G.W., 2006. Soluble Mn(III) in Suboxic zones. Science 313, 1955–1957. https://doi.org/10.1126/ science.1132876.

- Turner, R.E., 2022. Variability in the discharge of the Mississippi River and tributaries from 1817 to 2020. PLoS One 17, e0276513. https://doi.org/10.1371/journal. pone.0276513.
- Turner, R.E., Rabalais, N.N., Alexander, R.B., McIsaac, G., Howarth, R.W., 2007.
 Characterization of nutrient, organic carbon, and sediment loads and concentrations from the Mississippi River into the northern Gulf of Mexico. Estuar. Coasts 30, 273, 200
- Twining, B.S., Baines, S.B., 2013. The trace metal composition of marine phytoplankton. Annu. Rev. Mar. Sci. 5, 191–215. https://doi.org/10.1146/annurev-marine-121211-172322.
- Vanysek, P., 1992. Ionic Conductivity and Diffusion at Infinite Dilution. CRC Press.
- Viollier, E., Inglett, P.W., Hunter, K., Roychoudhury, A.N., Van Cappellen, P., 2000. The ferrozine method revisited: Fe(II)/Fe(III) determination in natural waters. Appl. Geochem. 15, 785–790. https://doi.org/10.1016/S0883-2927(99)00097-9.
- Wade, T.L., Soliman, Y., Sweet, S.T., Wolff, G.A., Presley, B.J., 2008. Trace elements and polycyclic aromatic hydrocarbons (PAHs) concentrations in deep Gulf of Mexico sediments. In: Deep Sea Res. Part II Top. Stud. Oceanogr., The Deep Gulf of Mexico Benthos Program, 55, pp. 2585–2593. https://doi.org/10.1016/j.dsr2.2008.07.006.
- Wang, Z.-W., Ren, J.-L., Jiang, S., Liu, S.-M., Xuan, J.-L., Zhang, J., 2016. Geochemical behavior of dissolved manganese in the East China Sea: seasonal variation, estuarine removal, and regeneration under suboxic conditions. Geochem. Geophys. Geosyst. 17, 282–299. https://doi.org/10.1002/2015GC006128.
- Webb, S.M., Dick, G.J., Bargar, J.R., Tebo, B.M., 2005. Evidence for the presence of Mn (III) intermediates in the bacterial oxidation of Mn(II). Proc. Natl. Acad. Sci. 102, 5558–5563. https://doi.org/10.1073/pnas.0409119102.
- Weiss, J., 2016. Handbook of Ion Chromatography, Fourth. ed. Wiley-VCH Verlag GmbH & Co. KGaA.
- Wen, L.-S., Santschi, P., Gill, G., Paternostro, C., 1999a. Estuarine trace metal distributions in Galveston Bay: importance of colloidal forms in the speciation of the dissolved phase. Mar. Chem. 63, 185–212. https://doi.org/10.1016/S0304-4203 (98)00062-0.
- Wen, L.-S., Shiller, A.M., Santschi, P.H., Gill, G., 1999b. Trace element behavior in Gulf of Mexico estuaries. In: Biogeochemistry of Gulf of Mexico Estuaries. Wiley, New York, New York, New York, pp. 303–346.
- Wen, L.-S., Santschi, P.H., Warnken, K.W., Davison, W., Zhang, H., Li, H.-P., Jiann, K.-T., 2011. Molecular weight and chemical reactivity of dissolved trace metals (cd, cu, Ni) in surface waters from the Mississippi River to Gulf of Mexico. Estuar. Coast. Shelf Sci. 92, 649–658. https://doi.org/10.1016/j.ecss.2011.03.009.
- Yakushev, E., Pakhomova, S., Sørenson, K., Skei, J., 2009. Importance of the different manganese species in the formation of water column redox zones: observations and modeling. In: Mar. Chem., 10th International Estuarine Biogeochemistry Symposium - "Estuaries in a Changing World", 117, pp. 59–70. https://doi.org/10.1016/j. marchem. 2009.09.007
- Yamashita, Y., Jaffé, R., 2008. Characterizing the interactions between trace metals and dissolved organic matter using excitation—emission matrix and parallel factor analysis. Environ. Sci. Technol. 42, 7374–7379. https://doi.org/10.1021/ es801357h.
- Yedema, Y.W., Sangiorgi, F., Sluijs, A., Sinninghe Damsté, J.S., Peterse, F., 2023. The dispersal of fluvially discharged and marine, shelf-produced particulate organic matter in the northern Gulf of Mexico. Biogeosciences 20, 663–686. https://doi.org/ 10.5194/bg-20-663-2023.